Comparison of the Synthesis and Heating Ability of Biofunctionalized Gold Nanoprisms and Nanorods for Bioapplications

Gabriel Alfranca Ramón

Supervisors:

Dr. Jesús Martínez de la Fuente

Dr. Scott G. Mitchell

June 2014

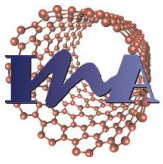

Instituto Universitario de Investigación
en Nanociencia de Aragón
Universidad Zaragoza

Universidad
Zaragoza

Index

Abstract

Gold nanoparticles (AuNPs) are particularly versatile and applicable nanomaterials, illustrated by many biomedical uses. Upon excitation of their localised surface plasmon resonance (LSPR) band, plasmonic NPs can undergo efficient light-to-heat transduction. NIR illumination of AuNPs is currently being explored in photothermal therapy optoacoustic imaging and very recently in thermal sensing. The LSPR bands of both triangular gold nanoprisms (*'nanonachos'* AuNNs) and gold nanorods (AuNRs) can be fine-tuned in the NIR range to exhibit strong absorption in the *'biological window'*. Upon excitation by incident light, photothermal conversion of the absorbed light energy generates an efficient and sharp local heating effect. Typically, these particular anisotropic AuNPs exhibit limitations relating to poor yield, unwanted by-products, the use of cytotoxic surfactants coupled with time-consuming syntheses. This thesis reports optimized high-yielding syntheses of biocompatible AuNNs and AuNRs in aqueous media whereby the LSPR band of both types of anisotropic nanoparticle can be fine-tuned from 800-1100 nm. The resulting colloidal AuNPs can be derivatised with heterobifunctional polyethylene glycol (PEG) to improve their colloidal stability, 4-aminophenyl β-D-glucopyranoside to enhance cellular uptake and the fluorescent dye TAMRA to verify the presence and location of the AuNPs inside cells. The heating properties of colloidal solutions of AuNNs upon illumination with a 1064 nm Class IV laser for 5 minutes were evaluated and compared to AuNRs. As a proof of concept, the biocompatibility and suitability of these functional AuNNs as photothermal agents was studied in cell cultures. Due to their ease of production, functionalisation, and remarkable heating features, the AuNNs appear to be overall more efficient particles than the AuNRs. Furthermore, the AuNNs represent a significant advance in the biocompatibility of nanoparticles and serve as an attractive alternative to those currently used as plasmonic photothermal agents.

1. INTRODUCTION AND BACKGROUND

1.1 General introduction to nanomaterials

Although the definition of nanomaterial sometimes lead to confusion significantly caused by an increasing wide variety of forms and compositions and their eclectic nature, the European Commission has defined it as *"a natural, incidental or manufactured material containing particles, in an unbound state or as an aggregate or as an agglomerate and where, for 50% or more of the particles in the number size distribution, one or more external dimensions is in the size range 1 – 100 nm"*. (Figure 1.1) This is a broad definition that covers a huge range of materials, including nanowires, thin films, surface coatings, organic nanoparticles and nanocrystals (inorganic-based nanoparticles).[1]

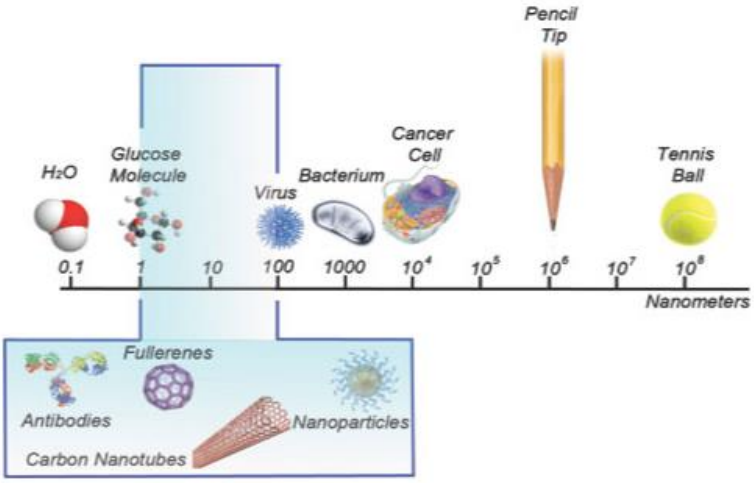

Figure 1.1 Overview of nanoscale location. Adapted from INL Institution webpage (INL.int).

Inorganic nanoparticles or nanocrystals reveal an array of fascinating physical properties (i.e superparamagnetism, surface plasmons or radiation-to-heat transduction) that are not present in bulk materials or at organic nanoparticles, and that make them interesting for a wide variety of applications in different scientific, technological and biomedical fields such as for diagnosis, drug delivery, imaging, treatment, theranostics, etc.. These nano-properties are determined by the chemical structure that leads to spatial confinements of their electrons, photons and electric fields due to size-dependence orbital structure variations of metals. Their large surface/volume is largely increased

[1] Types and uses of nanomaterials, including safety aspects 2012 Brussels, SWD(2012) 288.

that can be crucial in hardness, catalytic activity, and opto-electronic properties reactivity, among others.[2, 3]

Nanocrystals can be synthesized from a wide variety of different bulk materials as it is the case of noble metals (Au, Ag, Pt, etc.), metals (Rh, Ir, Ru, etc.), semiconductors (CdSe, CdS, ZnS, etc.), magnetic compounds (Fe_3O_4, Co, $CoFe_2O_4$, etc.) and several combinations of them (known as nanocomposites).[4] Every combination has its own properties, specific working conditions, limitations and applications, and such discussion is out with the scope of this thesis.

Although the term "inorganic" usually refers to the main structure that gives the nanoparticle its properties and characteristics, inorganic nanoparticles require a coating around their surface in order to prevent irreversible agglomeration due to van der Waals attraction, thereby resulting in an inorganic core surrounded by a polymer coating corona. Strategies of nanoparticle coating rely on the charge repulsion of a highly ionized coating which favours ionic dispersion; by using large polymers that prevents nanoparticles adsorption acting as steric hindrance; or resorting to a combination of both strategies [2]. It is also remarkable the fact that the coating can be ionically adsorbed or covalently coupled to the surface[5, 6], that makes nanoparticles respond differently to changes on the dilution in which they are suspended. NPs suspended in biological fluids will normally adsorb organic molecules, such as proteins, forming what is typically known as protein corona (See Section 1.3 for further details).[7]

[2] Ladj, R. *et al.* Individual inorganic nanoparticles: preparation, functionalization and in vitro biomedical diagnostic applications. *J. Mater. Chem. B* **1,** 1381 (2013).
[3] Scholes, G. D. Controlling the Optical Properties of Inorganic Nanoparticles. *Adv. Funct. Mater.* **18,** 1157–1172 (2008).
[4] Rao, C. N. R., Ramakrishna Matte, H. S. S., Voggu, R. & Govindaraj, A. Recent progress in the synthesis of inorganic nanoparticles. *Dalton Trans.* **41,** 5089–120 (2012).
[5] Zhang, F. *et al.* Polymer-coated nanoparticles: a universal tool for biolabelling experiments. *Small* **7,** 3113–27 (2011).
[6] Neoh, K. G. & Kang, E. T. Functionalization of inorganic nanoparticles with polymers for stealth biomedical applications. *Polym. Chem.* **2,** 747 (2011).
[7] Pino, P. del *et al.* Protein corona formation around nanoparticles – from the past to the future. *Mater. Horizons* **1,** 301 (2014).

1.2 Synthesizing nanostructures

Two different strategies are generally followed to obtain nanocrystals, so called "top-down" that resorts to physical methods such laser ablation and the "bottom-up" which employs solution-phase colloidal chemistry allowing to access to a variety of NPs sizes and shapes.[4, 8, 9]

How the atoms are packed into crystal structure is described by a model proposed by La Mer and coworkers[10], in which the precursor releases atoms to the reaction buffer until reaching a supersaturation state, moment in which the nucleation process takes place: those released atoms start to aggregate forming small clusters commonly known as nuclei. After nucleation, all clusters grow up until reaching a state in which fluctuations become so energetically costly that the cluster becomes locked into a well-defined structure, the so called "seed", whose structure determines the ultimate conformation and monodispersity of the final products. Seeds will grow into nanocrystals until an equilibrium state is reached between the atoms on the surface of the nanoparticle and the remaining atoms in solution.[9, 10]

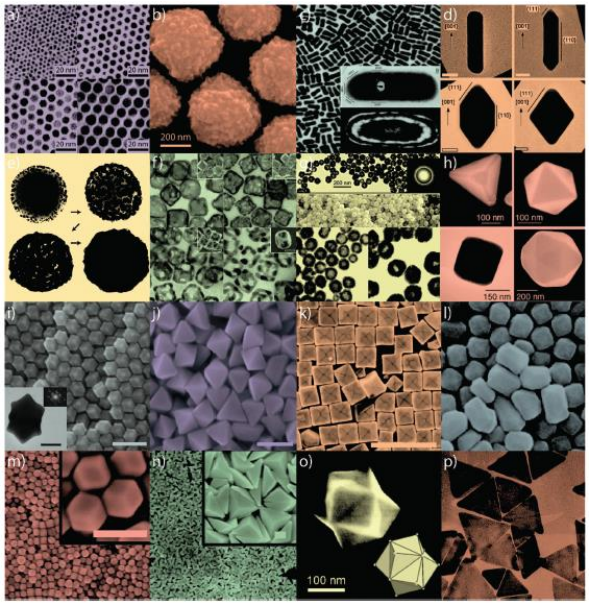

Figure 1.2 Some examples of nanoparticles that can be synthesized; adapted from El-Sayed[14].

The final shape resulting from the synthesis is determined by a combination of thermodynamic (*i.e.* temperature, reduction potential), kinetic factors (*i.e.* reactant concentration, diffusion, solubility concentration rate), as well as the presence and nature of capping agents[4,11]. Tuning the reaction conditions (*i.e.* by modifying seeds

[8] Pelaz, B. *et al.* Tailoring the synthesis and heating ability of gold nanoprisms for bioapplications. *Langmuir* **28,** 8965–70 (2012).

[9] Perez-Juste, J., Pastorizasantos, I., Liz-Marzan, L. & Mulvaney, P. Gold nanorods: Synthesis, characterization and applications. *Coord. Chem. Rev.* **249,** 1870–1901 (2005).

[10] Zaiser, E. M. and La Mer, V. K. The kinetics of the formation and growth of monodispersed sulfur hydrosols. *J. Colloid Sci.* **3,** 571–98 (1948).

[11] Shi, W., Casas, J., Venkataramasubramani, M. & Tang, L. Synthesis and Characterization of Gold Nanoparticles with Plasmon Absorbance Wavelength Tunable from Visible to Near Infrared Region. *ISRN Nanomater.* **2012,** 1–9 (2012).

structure or addition of several molecules), it is possible to access different shapes such as octahedral, tetrahedral, hexagonal plates, nanorods, triangular plates, dendrites, etc.[4,9,12] (Figure 1.2).

1.3 Interacting with biological systems

In the last decade, interest nanoscience has grown exponentially in relation to the study of different aspects of NPs in contact with living organisms and biomolecules. The main two reasons of this increasing interest are that NPs lie in the size range where most of bio-interactions occur, and that highly useful properties of materials have been described when reduced down to the nanoscale.[13, 14]

Bionanotechnology, or nanomedicine, was grown an increasing optimism with the general thought that this applied discipline can solve most of medical (therapy and diagnosis) and biology (sensing, limits of detection) issues, derived from the fact that huge diversity of applications in fields such as sensing, imaging, therapy or diagnosis was been described, sometimes with considerable high achievements.[2, 6, 14]

However, many challenges must be overcome, especially in the way nanoparticles interact with biological structures, mainly by their coating corona (surfactant or polymer) which ultimately determine their interaction with macromolecules, greatly influencing on the success of a particular nanostructure for a certain application.[6, 13, 15, 16]

Coating corona and/or nanoparticle surface are often modified by conjugation with several biological molecules, from peptidic structures (*i.e.* antibodies, enzymes), nucleic acids, carbohydrates, etc., as an attempt to give nanoparticles the required properties or by improving existing ones. Furthermore, any new nanomaterial has to be exhaustively studied when it comes in close contact with biological fluids and living cells or organisms, as unwanted nano-bio interactions may cause an unwilled unspecific effect, unexpected toxicity, loss of the desired properties of the nanoparticle or unexpectedly

[12] Yin, Z. *et al.* Construction of Stable Chainlike Au Nanostructures via Silica Coating and Exploration for Potential Photothermal Therapy. *Small* 1–6 (2014). doi:10.1002/smll.201400474

[13] Pelaz, B. *et al.* Interfacing engineered nanoparticles with biological systems: anticipating adverse nano-bio interactions. *Small* **9,** 1573–84 (2013).

[14] Dreaden, E. C., Alkilany, A. M., Huang, X., Murphy, C. J. & El-Sayed, M. A. The golden age: gold nanoparticles for biomedicine. *Chem. Soc. Rev.* **41,** 2740–79 (2012).

[15] Rabanel, J. M., Aoun, V., Elkin, I., Mokhtar, M. & Hildgen, P. Drug-loaded nanocarriers: passive targeting and crossing of biological barriers. *Curr. Med. Chem.* **19,** 3070–102 (2012).

[16] Moros, M. *et al.* The fate of nanocarriers as nanomedicines in vivo: important considerations and biological barriers to overcome. *Curr. Med. Chem.* **20,** 2759–78 (2013).

low half-life of the particles inside biological systems derived from *in vivo* processes, among other undesirable effects (Figure 1.3).[7, 13, 17]

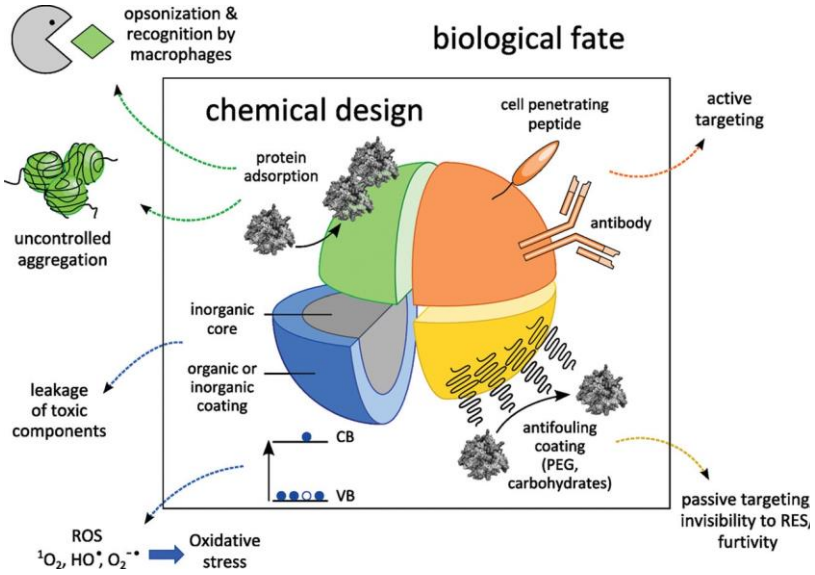

Figure 1.3 Some chemical designs of nanoparticles and already-described effects derived from interactions between nanoparticles and biological systems; reproduced from del Pino et al.[13]

Regardless of synthetic protocol, shape, size, surface area, roughness, porosity or crystal structure, arising structures from different functional groups (either from the coating surfactants or attached biomolecules) play a decisive role in the final bio-application, leading the way a nanomaterial interacts with macromolecules both in the media or in the organism (membrane receptors, chaperones, genetic material and so forth). Finally, it is important to highlight that when a NP comes in contact with a cell, what the cell senses is an unhomogeneous surface made of the functionalized molecules (and their corresponding functional groups) covering the inorganic core.[18, 19]

1.4 Optical hyperthermia for cancer treatment

Several examples of practical applications of various NPs such as nanorods, hollow nanospheres and nanostars, among others, are photothermal therapy (PTT), photoacoustic imaging or surface enhanced resonance spectroscopy (SERS), where NPs

[17] Sapsford, K. E. *et al.* Functionalizing nanoparticles with biological molecules: developing chemistries that facilitate nanotechnology. *Chem. Rev.* **113,** 1904–2074 (2013).
[18] Fratila, R. M., Mitchell, S. G., Del Pino, P., Grazu, V. & De La Fuente, J. M. Strategies for the biofunctionalization of gold and iron oxide nanoparticles. *Langmuir* (2014). doi:10.1021/la5015658
[19] del Pino, P., Mitchell, S. G. & Pelaz, B. Design and characterization of functional nanoparticles for enhanced bio-performance. *Methods Mol. Biol.* **1051,** 165–207 (2013).

can act as transducers. One of the most interesting novel applications of NPs is on cancer treatment by hyperthermia (or thermoablation).[14, 20, 21]

Hyperthermia is a very promising cancer treatment that has remarkable biological effect in tumor cells *in vivo.* It consists on the use of heat to kill and/or weaken tumor cells, making them more susceptible to be killed by other methods [20]. Although it is possible to directly kill carcinogen cells, clinical results have shown that the combination of radiotherapy-hyperthermia and chemotherapy-hyperthermia (thermochemotherapy) translates into a synergistic therapeutic improvement.[20, 21,22]

Two main mechanisms are major causes of these observations: firstly, hyperthermia has been reported to increase blood flow into the tumor; thus, an improved tissue oxygenation can prevent the hypoxic resistance and radio-sensitize the hypoxic area[20]; second, it has been demonstrated that also *in vitro*, where the hypoxic problem does not applies, hyperthermia improves radiation effects as well, probably caused by the result of destructive interference of the increased temperature with DNA repair after radiotherapy, by damaging cellular proteins.[20, 21, 23]

Although enhance of the cytotoxicity of many chemotherapeutic agents has been widely confirmed *in vivo*, cancerous cells are not inherently more susceptible to damage by heat than healthy ones. With the exception of hematological malignancies, normal and tumor cells are equally susceptible to increased temperatures *in vitro*, where the thermal energy dose required for induction of cell death in cell cultures appears to be related to the amount of energy to produce protein denaturation; it ultimately affects the cell by damaging structures like cytoskeleton, membranes, and enzyme complexes for DNA synthesis and repair. This energy dose required should carry the cell above a threshold temperature might vary between cell lines and in different stages of the cell cycle.[21]

Nevertheless, these studies contrast with *in vivo* results where tumor cells, in contrast to normal tissue, can be irreversibly damaged when exposed to temperatures between 40 and 44 °C; this is motivated by the characteristic physiology which most of types of

[20] Lal, S., Clare, S. E. & Halas, N. J. Nanoshell-enabled photothermal cancer therapy: impending clinical impact. *Acc. Chem. Res.* **41,** 1842–51 (2008).
[21] Dreaden, E. C., Mackey, M. a, Huang, X., Kang, B. & El-Sayed, M. a. Beating cancer in multiple ways using nanogold. *Chem. Soc. Rev.* **40,** 3391–404 (2011).
[22] Maestro, L. M. *et al.* Quantum dot thermometry evaluation of geometry dependent heating efficiency in gold nanoparticles. *Langmuir* **30,** 1650–8 (2014).
[23] Conde, J., de la Fuente, J. M. & Baptista, P. V. Nanomaterials for reversion of multidrug resistance in cancer: a new hope for an old idea? *Front. Pharmacol.* **4,** 134 (2013).

tumors share, as for instance the induced angiogenesis of solid tumors that results in chaotic non-efficient vessels where blood supply is therefore deficient[15,20], resulting in regions with hypoxia and low pH which ultimately makes cells more susceptible to hyperthermia treatment. With the exception of nerve tissues, this is normally not the case in non-tumor tissues, which remain unaffected even after an intense exposure.

It has been demonstrated that after hyperthermia treatment, a class of proteins called heat-shock proteins (HSPs) are expressed on the surface of tumor cells but not on the corresponding normal tissues. This wide variety of proteins, commonly regarded as chaperones, can also serve as cytokines that can stimulate the mononuclear phagocyte system (MPS), inducing dendritic cells and macrophages to produce pro-inflammatory cytokines and chemokines, and the consequent initiation of a nonspecific antitumor immunity. HSPs also serve as stress ligands, making tumor cells that express them on their surfaces more susceptible to lysis by natural killer cells. Finally, the release of HSPs following necrotic cell death stimulates the activation of antigen-presenting cells that can initiate a specific immune response against the tumor.[24]

However, suitable heat delivery and control represents a challenge, both from the technical and physiological point of view. This is caused primarily by the fact that none of devices currently available to apply hyperthermia therapies are able to destroy selectively a deeply situated cancer without destroying the surrounding healthy tissues.[21]

Nanotechnology can offer a wide variety of nanomaterials with great potential as ideal nanoheaters, together with the generation and control of non-ionizing radiation, which induces heat on the surface of nanoparticles[22]. Some examples are superparamagnetic NPs as well as plasmonic NPs that are currently investigated as nanoheaters or nanotransducers that can be remotely activated by radiation which do not (or minimally) interact with physiological tissue and fluids.[14, 18, 21]

Derived from an extraordinary development in recent years[14], this technology has provided us with complex nanomaterials not only with extraordinary physical properties but also with a vast array of molecules with of biological relevance such as antibodies, genetic material or tumoral markers of the most diverse nature, conferring

[24] Conde J, Ambrosone A, Sanz V, Hernandez Y, Marchesano V, Tian F, Child H, Berry C.C, Ibarra M.R, Baptista V.P, Tortiglione C, M de la Fuente J. Design of multifunctional gold nanoparticles for in vitro and in vivo gene silencing. *ACS Nano* **6,** 8316–24 (2012).

nanomaterials with complex functionalities including local heating, targeting (passive or active), improved uptake, delivery, biocompatibility, suitable biodistribution or non-immunogenicity, to name a few[18, 19]. Moreover, local heating by bio-active NPs can drastically reduce the side effects of radio and chemotherapies, allowing reducing effective dose. It must be acknowledged that another approach to destroy tumors implies directly NP-based heating, increasing the temperature above 46 °C and therefore, causing cell death by necrosis.[12, 14, 21]

This document is focused on the application and comparison of plasmonic-based NPs, as paramagnetic nanoparticles are out of the scope of this text. Thus, efforts were centered on producing plasmonic NPs that could act as nanoheaters for biomedical aplications.

1.5 Anisotropic Gold Nanoparticles as nanoheaters

Plasmonic nanoparticles (NPs) made of noble metals with well-defined shapes have received increasing attention due mainly to their unique optical properties and potential applications[1, 2, 14].

Among the wide variety of metallic NPs, gold nanoparticles (Au NPs) with a number of shapes such as pseudospheres, rods, cubes, or triangular prisms, to name a few, have found a great deal of interest in literature[8, 9, 14, 22, 24]. This generalized interest can be attributed to the characteristic properties of Au NPs including unique optical properties [3, 8, 9, 20-23], their biocompatibility, and ease of surface modification by a wide range of molecules[2, 6, 13, 18].

Firstly it is mandatory to set the basis on the concept of near infra-red (NIR) biological window. This range of frequencies covering from 1200 to ca. 750 nm correspond to a region where the absorptivity of biological systems is highly decreased, specially the contribution of cytochromes (*i.e.* hemoglobin) that lies in the visible region (see figure 1.4). This aspect allows light sources tuned to this range a harmless effect on life processes as well as a high penetration power towards biological structures[8, 21, 25].

[25] Huang, Y. Low-level laser therapy: an emerging clinical paradigm. *SPIE Newsroom* 2–4 (2009). doi:10.1117/2.1200906.1669

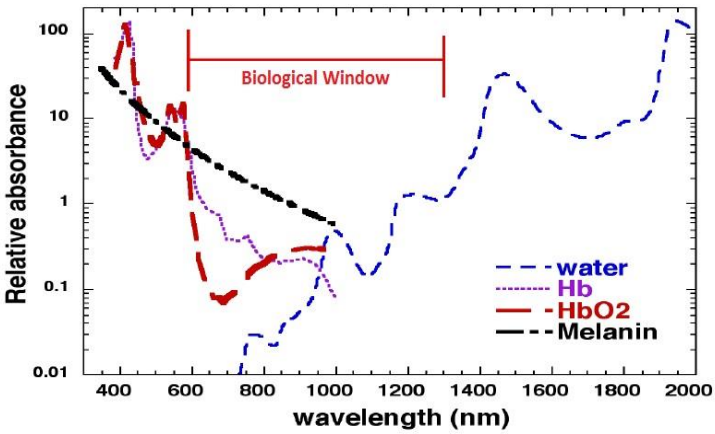

Figure 1.4 – EM spectrum representation with absorptivity spectra of water, hemoglobin (Hb), oxi-hemoglobin (HbO_2) and skin pigment melanin; adapted from Hamblin et al.[25]

The surface plasmon effect relates to coherent oscillations of conduction electrons on a metal surface excited by electromagnetic radiation at a metal–dielectric interface.[26] The optical properties of metallic structures are shown to be influenced primarily by the surface plasmon resonance (SPR) of conduction electrons, the frequency of which is determined by the nature of the metal, but is also sensitive to refractive index changes around the metal in combination with various other parameters, such as particle size and shape, the presence of a capping ligands, and even the dielectric properties of the surrounding medium[7, 8, 13, 14]. As a result, applications based on surface plasmon have attracted tremendous attention for its potential in optical sensing.[27] **Localized surface plasmon resonances** (LSPRs) are electromagnetic waves confined on metallic nanostructures.[28] LSPR of pseudospherical Au NPs (with a diameter < 100 nm) lies in the visible region of the EM spectrum and is responsible for their characteristic reddish color; here the main contribution to the position of the LSPR band is the diameter of the NPs. In general, for a greater NP diameter the LSPR band red-shifts[11]. Thus, when metal nanoparticles (NPs) of high symmetry are enlarged, their optical properties change only slightly, yet when an anisotropy contribution is added to the NP, such as growth of nanorods or nanoprisms, the optical properties of the nanoparticles change dramatically and are typically highly size-dependent.[11, 29] As a result, in such types of anisotropic nanoparticles the major

[26] Liz-Marzán, L. M. Tailoring surface plasmons through the morphology and assembly of metal nanoparticles. *Langmuir* **22,** 32–41 (2006).
[27] Mayer, K. M. & Hafner, J. H. Localized surface plasmon resonance sensors. *Chem. Rev.* **111,** 3828–57 (2011).
[28] Stewart, M. E. *et al.* Nanostructured plasmonic sensors. *Chem. Rev.* **108,** 494–521 (2008).
[29] a) Eustis, S. & el-Sayed, M. A. Why gold nanoparticles are more precious than pretty gold: noble metal surface plasmon resonance and its enhancement of the radiative and nonradiative properties of nanocrystals of different shapes. *Chem. Soc. Rev.* **35,** 209–17 (2006); b) Li, N., Zhao, P. & Astruc, D. Anisotropic gold nanoparticles: synthesis, properties, applications, and toxicity. *Angew. Chem. Int. Ed. Engl.* **53,** 1756–89 (2014).

contribution to the UV−vis/NIR spectrum corresponds to the in-plane dipolar mode laying in the NIR range.[8]

The optical properties of metallic NPs are therefore mainly dictated by their LSPR band, which for NPs made of noble metals, it lies in the visible/NIR part of the spectrum. NIR band of Au NPs can be excited to produce heat very efficiently, leading NIR excitation of noble metal NPs as the most favorable scenario for biomedical applications[14, 21]. Light-to-heat conversion can be used to design applications, such as hyperthermia and drug release, where anisotropic Au NPs act as nanoheaters that can be remotely triggered by NIR radiation. To date, some approaches have shown successful results in remote ablation of tumors, as the case of Au nanorods and hollow nanocages in the treatment of tumors in mice.[8]

Nevertheless, many of the methods to produce NIR absorbing Au NPs rely on challenging syntheses with several complex steps and/or seed-mediated approaches involving the cationic surfactant cetyltrimethylammonium bromide (CTAB)[4, 8, 9, 11, 12]. CTAB is said to be the most widely used and convenient surfactant for high-yielding syntheses of Au nanorods[11] and nanoprisms[8]. However it is a well-known highly toxic component, and thus methods to exchange CTAB for other less cytotoxic surfactants or polymer coatings have been extensively reported[5, 8, 9, 11-13, 24]. In conclusion, an alternative method to produce NIR absorbing Au NPs without CTAB is of the most importance, as recently highlighted by Murphy and coworkers, pioneering author of the seed-mediated approach involving CTAB[8, 29].

To sum up, **Gold nanoparticles** (AuNPs) represent a particularly versatile and applicable type of nanoparticle, illustrated by recent developments that have exploited **AuNPs as biolabels taking advantage of their optical properties**, i.e. surface plasmons yield very high extinction coefficients, *ca.* $3x10^{11}$ $M^{-1}cm^{-1}$ (two orders of magnitude larger than that of common fluorophores), and high electric fields in the most immediate vicinity of plasmonic NPs.[30] Moreover, **upon excitation of their plasmon**

[30] a) Haes, A. J., Zou, S., Schatz, G. C. & Van Duyne, R. P. Nanoscale Optical Biosensor: Short Range Distance Dependence of the Localized Surface Plasmon Resonance of Noble Metal Nanoparticles. *J. Phys. Chem. B* **108,** 6961–6968 (2004); b) Near, R. D., Hayden, S. C., Hunter, R. E., Thackston, D. & El-Sayed, M. A. Rapid and Efficient Prediction of Optical Extinction Coefficients for Gold Nanospheres and Gold Nanorods. *J. Phys. Chem. C* **117,** 23950–23955 (2013).

band, **plasmonic NPs can undergo efficient light-to-heat transduction.**[31] NIR illumination of AuNPs is currently being explored in photothermal therapy,[32] imaging (thermal[33] and optoacoustic imaging[34]) and very recently in thermal sensing. Remarkably, the efficiency of AuNP colloidal solutions to drive **light-to-heat conversion** is close to 1: although heating with a single NP is limited by its absorption cross section, the intensity of the laser source and equilibrium distribution of temperature increase around the NP.[35]

Above many other potential applications, a wide variety of methodologies are published describing various types of anisotropic Au NPs that would potentially be applied in future optical hyperthermia therapies in fighting against cancer, some of which require deeper study and must be compared to well established techniques to determine their potential capability to be applied in a future[8, 11, 12, 14, 20, 21, 29, 31, 32]. Both **triangular gold nanoprisms** (AuNPrs)[8] and **nanorods** (AuNRs)[36] exhibit strong absorption in the NIR range and **upon light excitation**, **sharp local heating** can be generated by the photothermal conversion of the absorbed light energy into local heating through a non-radioactive mechanism, rendering these particular anisotropic AuNPs as extremely efficient for NIR-radiation-induced heating and specially in laser- coupled thermoablation (Figure 1.5).[8, 20, 37]

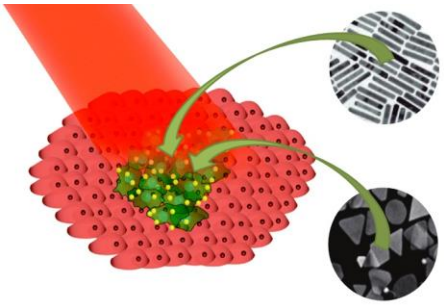

Figure 1.5 Both NRs and NPrs can eventually induce cell death by producing local heating while being irradiated with NIR light adjusted to their LSPR wavelength [8], [20] and [37].

[31] Jiang, K., Smith, D. A. & Pinchuk, A. Size-Dependent Photothermal Conversion Efficiencies of Plasmonically Heated Gold Nanoparticles. *J. Phys. Chem. C* **117,** 27073–27080 (2013).

[32] a) 1. Huang, X., Jain, P. K., El-Sayed, I. H. & El-Sayed, M. A. Plasmonic photothermal therapy (PPTT) using gold nanoparticles. *Lasers Med. Sci.* **23,** 217–28 (2008).; b) Choi, W. Il *et al.* Tumor regression in vivo by photothermal therapy based on gold-nanorod-loaded, functional nanocarriers. *ACS Nano* **5,** 1995–2003 (2011).

[33] Baffou, G. *et al.* Thermal imaging of nanostructures by quantitative optical phase analysis. *ACS Nano* **6,** 2452–8 (2012).

[34] Bao, C. *et al.* Gold nanoprisms as optoacoustic signal nanoamplifiers for in vivo bioimaging of gastrointestinal cancers. *Small* **9,** 68–74 (2013).

[35] Richardson, H. H., Carlson, M. T., Tandler, P. J., Hernandez, P. & Govorov, A. O. Experimental and theoretical studies of light-to-heat conversion and collective heating effects in metal nanoparticle solutions. *Nano Lett.* **9,** 1139–46 (2009).

[36] Liu, J. *et al.* Gold nanorods with phase-changing polymer corona for remotely near-infrared-triggered drug release. *Chem. Asian J.* **9,** 275–88 (2014).

[37] Vigderman, L., Khanal, B. P. & Zubarev, E. R. Functional gold nanorods: synthesis, self-assembly, and sensing applications. *Adv. Mater.* **24,** 4811–41, 5014 (2012).

2. OBJECTIVES

The gran aim of the research carried out in the group of **Dr. Jesus Martínez de la Fuente** at the **Instituto de Nanociencia de Aragón** is the development of novel functional nanomaterials for biotechnological applications with a particular focus on sensing and therapy.

The objectives of this Masters Thesis entitled *'Comparison of the Synthesis and Heating Ability of Biofunctionalized Gold Nanoprisms and Nanorods for Bioapplications'* is to identify, synthesize, characterize and functionalize two distinct types of gold nanoparticles (AuNPs) then study and compare their stability in cell media, their internalization within cells and finally their behaviour under irradiation from NIR laser light.

Excitation of the localised surface plasmon resonance (LSPR) band of plasmonic AuNPs can produce efficient light-to-heat transduction leading to a sharp heating effect. Since the LSPR bands of certain AuNPs can be fine-tuned in the NIR range to exhibit strong absorption in the *'biological window'* these types of particles can be employed in biosensing, optoacoustic imaging and photothermal therapy. The overall aim of this thesis centres on producing biocompatible AuNPs in aqueous media possessing LSPR bands in the range 800-1100 nm before functionalizing their surfaces with biomolecules to enhance cellular uptake and dyes which serve as biomarkers. The heating properties of the resulting biofunctionalized AuNPs upon illumination with a 1064 nm Class IV laser will be evaluated. Thereafter, the stability and behaviour of the particles in cell culture media will be assessed before performing proof of concept *in vitro* cell internalization and heating studies.

3. RESULTS AND DISCUSSION

3.1 Synthesis and characterization of nanoparticles

3.1.1. Synthesis of Triangular Gold Nanoprisms ('Nanonachos', NNs)

Two different straightforward aqueous synthetic routes were used to obtain gold nanonachos (NNs) in a variety of sizes, thereby allowing a comparison of their optical characteristics and other size-related effects. These routes are high yielding syntheses performed at room temperature and avoid the use of highly toxic reagents. For this work, a previously reported procedure[8] was used to obtain NNs with an LSPR band centred at 900 nm and with 73±12 nm per side, herein referred as "standard protocol" or simply "900 nm protocol"; while a modified version of this route was employed to access NNs with an LSPR band at 1064 nm and 286±48 nm per side, which was called "enhanced protocol" or "1000 nm protocol". To obtain NNs with an LSPR band at 900 nm, sodium thiosulfate $Na_2S_2O_3$ (aq) (STS) was used as a mild reducing agent for gold salt chlorauric acid $HAuCl_4$. STS was added slowly to a solution of Au(III) ions and allowed to reacted untouched for a period of 9 min, allowing the first NNs 'seeds' to form; thereafter a second volume of STS was added and the solution was allowed to sit, undisturbed for 60 min to complete the formation of colloidal particles of Au NNs.

NNs with an LSPR band centred at 1064 nm, so called enhanced protocol, were synthesized using a minor modification of the aforementioned route. To produce these larger NNs, a small amount of potassium iodide, KI (1.32 mM final concentration) was added to the first STS solution; a second addition of STS+KI was performed 4 min before the reaction has started, and after another 4 min the reaction was stopped the same way as for the 900 nm NNs. The mixture was left undisturbed for 60 min, after which time the UV-Vis spectrum revealed a strong absorbance peak at *ca*. 530 nm and another peak at the NIR region centred at 1064 nm. Subsequent electron microscopy analysis revealed these to correspond to pseudo-spherical polyhedral gold nanoparticles (NSs) and NNs, respectively (Figure 3.1).

To further increase the colloidal stability of the nanoparticles, all the reaction products were derivatized with heterobifunctional polyethylene glycol (HS-PEG-COOH, MW = 5000 g/mol (5 kDa)). The increased colloidal stability allowed us to separate NNs from Au NSs and from other by-products by centrifugation. The required amount of PEG was obtained applying an empirically demonstrated correlation of the amount of gold in the NPs ensuring that an excess of the former is added to the NNs solution in order to obtain properly covered and stabilized NNs. A conversion factor was obtained previously from a correlation of the intensity of the LSPR band from the UV-vis spectrum and the quantity of gold determined by ICP analysis. Consequently, using the intensity of the LSPR band absorbance from the UV-Vis spectrum and

applying a conversion factor (Ɛ) 25 mL mg^{-1} cm^{-1} it was possible to obtain the concentration (mg/mL) of gold NNs in the sample. Calculating the total quantity of NNs, it was possible to estimate an excess amount of PEG required. This amount was empirically calculated for each PEG molecule, half the amount of NNs in mg in this case, with a margin of error sufficient to ignore the presence of spheres and other gold aggregates. To avoid the formation of S-S bonds between individual PEG molecules (PEG dimers) sodium borohydride, $NaBH_4$, was required as a reducing agent at a molar ratio of 1:1 with PEG at pH 12.0. The PEG stabilization of the NNs was carried out under sonication of the mixture at 60 ºC for one hour to speed-up the process, and as an alternative to the over-night incubation under mild mixing[8].

The final volume was centrifuged in order to separate unreacted reagents and pseudo-spherical (herein polyhedral) Au crystals. The red-coloured supernatants from these centrifugation steps were discarded, even though UV-Vis of supernatants show that a minor amount of NNs are lost at each purification step; most likely smaller and lighter particles, as they revealed slightly lower LSPR values (*ca.* 800 nm in the case of standard protocol and *ca.* 990 nm from enhanced protocol) (Figures 3.1 and 3.2). From collected pellets new spectra and SEM still revealed an LSPR band at *ca.* 550 nm and the presence of polyhedral Au NSs. In order to separate the polyhedral particles from NNs, samples were diluted to ¼ of their volume and aliquoted in 50 mL centrifuge tubes to let them decant at room temperature for several weeks. This way, pseudo-spheres, smaller nanoparticles and other pollutants remain at the top of the centrifuge tube where they can be easily removed using a pipette, while NNs sediment at the bottom of the recipient.

Although NNs obtained from this method are considered to be stable enough, the stability of each batch of sample should be tested before use by preforming UV-Vis spectroscopy and SEM as described. Any shifting of LSPR peak, intensity or shape changes should be taken into account since these optical characteristics are direct markers of any aggregation or degradation of the NPs.

After synthesis was finished, the ratio between NNs LSPR peak and the polyhedral Au nanoparticles (NSs) should be close to 1.8 to ensure that the synthesis has sufficient quantity and quality to meet the needs of our studies. NNs produced using each of the aforementioned protocols were characterized using both UV-Vis and SEM (Figures 3.1 and 3.2). Two days after synthesis, the ratio of NN:NS in 900 nm LSPR NNs was 1.8; while in the case of 1050 nm NNs the ratio of NNs to NSs was slightly higher and reached 2.0. Consequently, although the yield of the synthesis and formation of NNs in both cases is high, the described 1050 nm protocol produced slightly more NNs than the literature reported procedure.

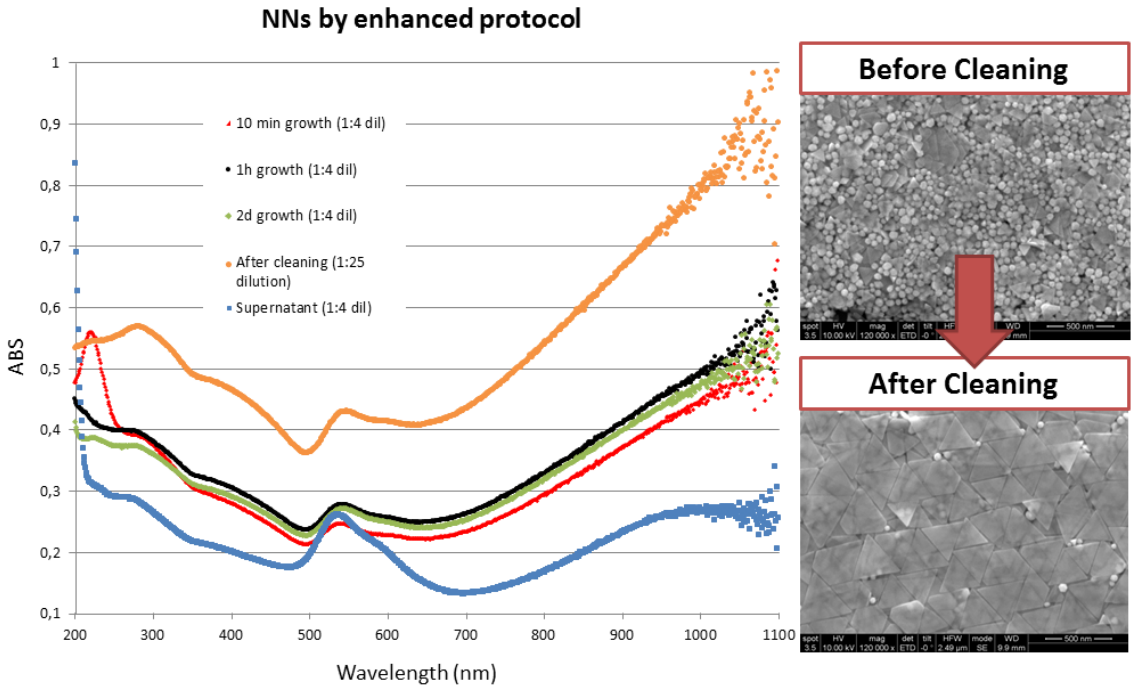

Figure 3.1 Left: spectra evolution throughout the synthesis; 2 days after growth spectrum (green) was performed to check NNs stability; supernatant revealed the presence of some prism-shaped structures lost during the process; last cleaning step was measured 25 times more diluted than all other steps. Right: SEM images after and before cleaning process; note that although the process is able to discard most of NSs, the resultant sample of NNs still has a small proportion of NSs.

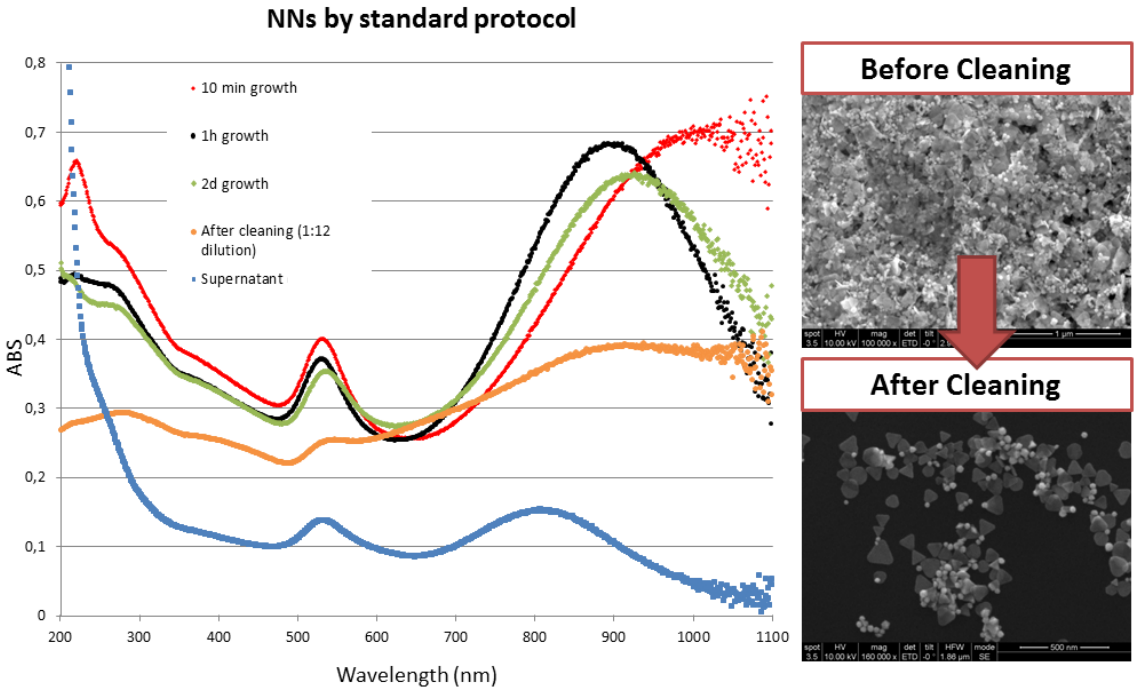

Figure 3.2 Same specifications as for figure 3.1, this time applied to standard protocol. Left: Note that although first minutes of synthesis are able to form NNs with LSPR close to 1000, they rapidly blue-shift to longer wavelengths; after-cleaning solution was loaded 12 times more diluted than the others. Right: before and after cleaning process, revealing that a vast majority of NSs were removed.

3.1.2 Synthesis of Gold Nanorods (NRs) with LSPR <850 nm

A seed-mediated growth process was applied for all synthetic procedures. These first approaches were based on Liang-Tang – El-Sayed studies[11, 38] that described two different protocols: a CTAB-based protocol and a dual surfactant mixture (consisting of CTAB/BDAC at an specific molar ratio). Both methods were performed in our studies, together with several modifications and optimization attempts.

A seed solution was first prepared by adding $NaBH_4$ as a reducing agent to a CTAB/$HAuCl_4$ solution under rapid mixing and left undisturbed for 1-2 hours. This step was common to all LSPR <850 nm NRs protocols, and was also similar to Zurbarev's method[11] (described in detail in next section). The brown-coloured solution that was obtained contained small pseudo-spherical nanoparticles (diameter *ca.* 3 nm) that subsequently served as seeds during NR growth synthesis.

Track exp	LSPR (nm)	Variations
NR-A1	690	300 uL $AgNO_3$ and 480 uL seed sol.
NR-A2	-	150 uL $AgNO_3$ and 480 uL seed sol.
NR-A3	620	300 uL $AgNO_3$ and 96 uL seed sol.
NR-A4	620	300 uL $AgNO_3$ and 300 uL seed sol.
NR-A5	600	300 uL $AgNO_3$ and 96 uL seed sol.
NR-B1	672	CTAB/BDAC added to seed sol.
NR-B2	676	Standard protocol
NR-B2a	-	Additional $HAuCl_4$ after synth. starts
NR-B2b	667	Add. growth sol. after synth. starts
NR-B3	680	Standard protocol

Table 3.1 List of experiments performed, LSPR values obtained and variations and/or conditions of the reactions.

For both methods, several centrifugation-washing steps were required after each reaction to clean NRs from excess of surfactants. It is important to note that different configuration conditions were used as these washing steps often caused changes in the plasmon resonance of the NRs as a result of alterations in the shape, aspect ratio and state of aggregation of the NRs[11]. In such a way, the stability of NRs could be studied as a function of the different centrifuge speed and times. Furthermore, for both methods several variables were also modified to investigate the influence of each one on the yield, size and LSPR band of the NRs in an attempt to tune the LSPR to longer wavelengths to match the wavelength of the Classs IV laser (1064 nm) to be used for NIR application. See Table 3.1 for further details.

[38] Nikoobakht, B. & El-Sayed, M. A. Preparation and Growth Mechanism of Gold Nanorods (NRs) Using Seed-Mediated Growth Method. *Chem. Mater.* **15,** 1957–1962 (2003).

3.1.2.1. CTAB-based trials

For first trials, the CTAB single surfactant solution was used. CTAB was added to a $HAuCl_4$ solution that was subsequently reduced firstly with an appropriate volume of $AgNO_3$ solution and followed by the addition of ascorbic acid (AA). A determined volume of previously prepared seed solution was then added to the colorless growth solution, initiating NR synthesis. Seeded-growth solutions were aged overnight and monitored by UV-Vis spectroscopy. Herein, several concentrations of silver nitrate and seed addition were tested, as they are established as the most effective players in precise control of rod shape and size[11] and thus influencing the final aspect ratio.[9]

The CTAB-based method was firstly labeled "**NR-A1**" and performed by reproducing the literature conditions: 300 µL of $AgNO_3$ and 480 µL seed solution were used as this is the maximum amount added following the literature that should give the highest aspect ratio[11]. Higher than these amounts, the yield would decrease, other shapes would be produced at higher amounts and/or LSPR would shift to shorter wavelengths[9, 11, 38]. After overnight aging two centrifugation steps were performed at room temperature (8000 rpm/30 min) and the precipitated colloids were resuspended in Milli-Q water. Once all surfactants were washed away, UV-Vis spectra were collected and samples were stored at room temperature. SEM images were collected prior to washing (Figure 3.3) that gave low resolution due to presence of high amounts of surfactant. Under these conditions samples revealed plasmon wavelengths that corresponded to NR formation (*ca.* 690 nm) that is, however, too short for our purposes. Nevertheless, the synthetic method successfully produced NRs, and the procedure was further optimized. Reported literature method ages growth solution for a maximum time of 25 days, and it is established that growing times up to 10 days may be sufficient to produced fully growth NRs with LSPR at the NIR region. The longer LSPR wavelengths are said to be reached after the first two weeks, and starting decreasing since then[11]. For these reasons samples were followed from 8 to 14 days aging time in most cases. In this case samples were followed during the maximum growth time, but no relevant improvements were delivered from their optical properties, as LSPR peak was arrested at *ca.* 690 nm (Table 3.1).

After this first approach, the influence of $AgNO_3$ and of seed solution addition were studied by performing two different trials (named **NR-A2** and **NR-A3**) using 150 µL $AgNO_3$ and 480 µL seed solution, and 300 µL $AgNO_3$ and 96 µL seed solution respectively. 150 µL $AgNO_3$ were added in order to ensure that high concentrations of silver were not influencing negatively on the LSPR wavelength within the previously added seed volume. On the other hand, an amount of 96 µL seed solution was used based on the standard protocol performed in the bibliography[11]; therefore, this amount was used as an attempt to exactly know how the silver affects NR

growth. Both experiments were seeded at the same time using a common seed solution. Samples were monitored by UV-Vis spectra.

After three days aging, while monitoring, **NR-A2** UV-Vis revealed no NR production, and plasmon wavelength of **NR-A3** was at *ca.* 620 nm, revealing a blue-shift compared with **NR-A1** (*ca.* 690 nm). In addition, both **A2** and **A3** experiments, as well as their corresponding seed solution produced vast quantities of macroscopic CTAB crystals due to the high concentration of CTAB in solution. Crystal growth can be exacerbated by an improperly performed CTAB suspension during stock preparation and/or the absence of a sonication step to aid dissolution. This is not the case with experiment **NR-A1**, which remained soluble during almost the whole aging process, probably because variations on room temperature during the growth time required by the synthesis or more likely due to a much lower surfactant concentration, revealing the importance of a homogeneous fully dissolved CTAB solution, that is hard to obtain at such high concentrations, and was finally achieved by sonicating CTAB stock solutions for a few seconds at 40 ºC until solution became colourless. As a result of this observation, all subsequent synthetic procedures included a sonication step as part of CTAB stock solutions preparation. In order to save samples from crystal formation, supernatants were separated from aggregated crystals and the aggregated NPs were discarded. The remaining volume was heated (65 ºC) while shaking (800 rpm) until any possible remaining crystals were soluble again. The presence of NRs was confirmed by UV-Vis of the supernatant resuspended in water. This method was used for all samples that showed crystal formation saving a significant part of NPs.

After homogenization of sample, **NR-A3** was washed by centrifugation as described. Three centrifugation steps were performed at room temperature (1º 5500 rpm/30 min; 2º 9000 rpm/15 min; 3º 8000 rpm/15 min). The reason why a weaker centrifugation step was performed in the first place is because it was noticed that strong centrifugation steps would induce surfactant precipitation, as pellets contained CTAB and washing did not properly clean surfactant from samples. For this reason, lower rates of centrifugation (e.g. 5500 rpm) were used for the first washing step, which allowed NRs to form cleaner pellets as CTAB remained at the supernatant. After this first step most CTAB was washed from the sample and centrifugation steps could be performed under stronger conditions (e.g. 8000 rpm) that would reduce NRs loss during washing. Once all of the surfactant was removed by these washing steps a UV-Vis spectrum was collected, obtaining the same value as previously reported (*ca.* 620 nm), and the sample was kept at room temperature. After several days, **NR-A3** appeared aggregated and precipitated; sonication was not enough to resuspend NRs and eventually the experiment was discarded. Finally, UV-Vis and SEM were performed for washed **NR-A2** revealing the presence of irregular nanoparticles with undefined shapes, mostly pseudo-spheres from different sizes (Figure 3.3), probably derived from the decrease

In principle, these experiments permitted the synthesis of NRs. However, several factors rendered these unsuitable for our studies, namely low yield, irregular NRs shape, shorts LSPR band wavelengths and several vicissitudes were found during the process and for sample stabilization. Furthermore, the reproducibility of the experimental procedures[9, 11, 38] was often questionable and should be checked. As a last attempt to improve these aspects of the method, two more trials were performed: **NR-A4** and **NR-A5**.

NR-A4 was performed using 300 µL of $AgNO_3$ and 300 µL seed solution similar to **NR-A1** (300 and 480 µL respectively) with improvement purposes. **NR-A5** was a repetition of previously performed **NR-A3** (300 µL $AgNO_3$ and 96 µL seed), in order to obtain stable nanoparticles that were observed by SEM. For both **A4** and **A5** experiments, fresh $AgNO_3$ stock solution was prepared and protected from light to discard that the reason of the low aspect ratios obtained from previously performed experiments were caused by the depletion of silver caused by the precipitation of the stock solution. During the whole process both experiments were monitored by UV-Vis spectra and compared with all other CTAB-based experiments (Figure 3.3; Table 3.1). CTAB crystals appeared once again in both samples and a cleaning protocol was performed to separate crystals from supernatant. Afterwards, just like previous experiments, **NR-A4** and **NR-A5** were washed by centrifugation. Three centrifugation steps were performed at room temperature. **NR-A4** was centrifuged 2 times at 8000 rpm 30 min and NR-A5 was firstly centrifuged at 5500 rpm 30 min once, followed by another two steps (8000 rpm for 30 min). When all excess surfactant had been removed, UV-Vis spectra were obtained and samples were stored at room temperature. As a result, it was confirmed that strong centrifugation steps would induce surfactant precipitation, as pellets contained CTAB and washing did not properly clean surfactant from samples. SEM images of **NR-A4** and **NR-A5** experiments showed clear and surfactant-free rod-like nanoparticles, but with extremely low aspect ratios that was supported by UV-Vis (Figure 3.3).

NR-A1 was performed using the maximum amount of $AgNO_3$ and seed solution described by the literature, and was able to reach a maximum plasmon resonance at 690 nm. **NR-A2** revealed the presence of NRs in at a very low yield, and its LSPR was not detected by UV-Vis, demonstrating that depletion of Ag with an increased amount of seed solution does not produce NRs at a correct size and shape homogeneity. However **NR-A3** with a high amount of Ag (addition of 300 µL $AgNO_3$) was able to produce NRs, but decreasing amount of seed solution leads to lower plasmon resonances (620 nm). Two final experiments, **NR-A4** and **A5** showed plasmon resonances of 622 nm and 601 nm respectively before centrifugation; considering that after centrifugation, plasmon wavelength blue-shifts[9, 11, 39], no improvement was shown compared with previous attempts.

3.1.2.2. CTAB/BDAC-based trials

After those first approaches, and as a variation to the single surfactant method (CTAB), the two-surfactant (CTAB/BDAC) growth solution was used at a molar ratio of 2.77 as described in the literature[11]. This ratio was described as optimum to obtain the longest aspect ratio of the NRs that directly gives a red-shifting close to the NIR region required of the colloidal particles for this study. The combination of CTAB and BDAC as surfactant agents would theoretically allow us to produce NRs with a plasmon wavelength higher than 900 nm within a few hours growth time[11, 39], which was not the case. Due to the longer growth periods samples were aged from 2 to 11 days and their growth was monitored by UV-Vis spectroscopy, followed by several washing steps and SEM images collection. For a proper washing of samples, an additional centrifugation-washing step should be included at first place with stronger conditions (6-7000 rpm) to allow NRs to precipitate due to high viscosity of CTAB/BDAC mixture.

For these CTAB/BDAC-based trials, the seed solution was firstly made by two different methods for two different experiments at the same time named **NR-B1** and **NR-B2**; **B2** was prepared as described for the CTAB-based method and **B1** was made substituting CTAB by a CTAB/BDAC mixture at the same molar ratio and final concentrations as for growth solution. Both experiments were performed and monitored simultaneously and resultant NRs were characterized at same conditions. Both experiments were monitored for 13 and 11 days respectively using UV-Vis spectroscopy. There was evidence of a minor shift of *ca.* 20 nm in the process, as they revealed LSPR at *ca.* 674 nm for **NR-B1** and 676 nm for **NR-B2** compared with previous results (Figure 3.4). The former revealed some aggregates that were resuspended easily by sonication for some seconds. Resuspended fraction of **NR-B1** was treated separately and washed differently to decrease NR loss as much as possible: 6500 rpm 30 min followed by 3 steps at 5500 30 min for B1, and 7000 rpm 30 min followed by 3 steps at 5500 for 30 min for its resuspended fraction. After ensuring that UV-Vis spectra and SEM images were similar to non-aggregated fraction, both samples were mixed together and used as equals. SEM revealed the fractions to have the same irregular rod shape, revealing that no neither the process nor the lightly different centrifugation conditions affect the final product.

As a last attempt to increase NRs length, and following the literature[9, 11], six days aged **NR-B2** was divided in two and additional gold and growth solution were added to each volume: **NR-B2a** was added to 1 mL $HAuCl_4$ 1mM and **NR-B2b** was added to a proportional volume of growth solution (500 µl BDAC/CTAB; 20 µL $AgNO_3$ 4 mM; 300 µL $HAuCl_4$ 1 mM and 7 µL ascorbic acid 78 mM). Immediately after gold addition, B2a sample apparently produced spheres, with no NRs growth as LSPR band at 678 nm disappeared. Unexpectedly, B2a sample produced some irregular prism-shaped forms revealed at SEM after wash (Figure 3.3). B2b

sample was aged for 13 days incubation period (seven more days) but revealed no further progress, as it kept the LSPR peak at approximately same wavelength as before addition. B2a was washed using three centrifugation steps at 6500 rpm for 30 min. To wash surfactants from sample B2b, a 7000 rpm centrifugation for 30 min was required in the first place to remove most of excess of surfactant, followed by three more centrifugation steps at 5500 rpm during 30 min with the intention to avoid as much as possible the decrease observed in the aspect ratio due to stronger centrifugation conditions described in the literature and proved by our studies[9, 11]. UV-Vis and SEM images were obtained from both final samples before being stored at room temperature (Figure 3.3).

Further illustrating the irreproducibility of the Liang-Tang method, one final attempt at the synthesis was performed (**NR-B3**). All protocol steps were identical to the protocol description. The seed solution was prepared the same way as for **NR-B2** and after overnight aging, the wavelength of the LSPR band reached values similar to experiments NR-B1 and B2 after six days aging (*ca.* 680 nm). However, it should have been higher than 800 nm according to the literature[11]. **NR-B3** was washed the same way as NR-B2 and UV-Vis revealed an LSPR band at 670 nm after washing. Both SEM and TEM images were recorded from **NR-B3** sample and histograms were obtained. It was clearly observed the existence of two separate populations of samples: one corresponding to short nanorods and another that implies the presence of big pseudo-spheres; these two species are observed in all other experiments, revealing that this protocol leads with the formation of alternative undesirable gold conformations (Figure 3.5).

NR-B1 and **B2** revealed LSPR of 674 and 676 nm respectively, and additional growth solution added to the sample (**NR-B2b**) did not improve wavelength of the plasmon band. Moreover, the addition of extra $HAuCl_4$ (**NR-B2a**) leads NRs to form irregular NNs. The final experiment, **NR-B3**, did not provide a plasmon wavelength bellow than 670 nm that did not implies a significant improvement compared with CTAB-based experiments. Consequently, the results obtained revealed that neither the CTAB protocol nor the BDAC/CTAB method were capable of producing NRs with LSPR higher than 700 nm.

From these reactions it is clear that CTAB exerts a great influence on the outcome of the reaction. Therefore, the influence and manipulation of CTAB, variables such as seed addition, the presence of Ag, additional volumes of solvent added during aging as well as the aging times radically affect the resultant NRs.

In summary, these reported experimental procedures provide unreliable routes towards Au NRs with length:breadth ratio of 3.28 ± 1.47 (data collected from **NR-B3** experiment), which high deviation values are primarily caused by the growth of pseudo-spheres together with NR

formation, corresponding to an aspect ratio around 1 and SPR of *ca.* 550 nm. Since our research required Au NPs with an LSPR band centred as close to 1064 nm as possible, these synthetic protocols were of little use due to their poor reproducibility, long incubation times, arduous synthetic step, laborious stabilization of the particles and very sensitive synthetic conditions in which any change in variables like temperature, small changes of concentration of the reducing agent, amount of silver added, seed/Au ratio and washing conditions, lead to the conclusion that this protocols are definitely not practical to obtain long aspect ratio NRs at a very high yield that may be the optimal nanoparticles for hyperthermia studies[39].

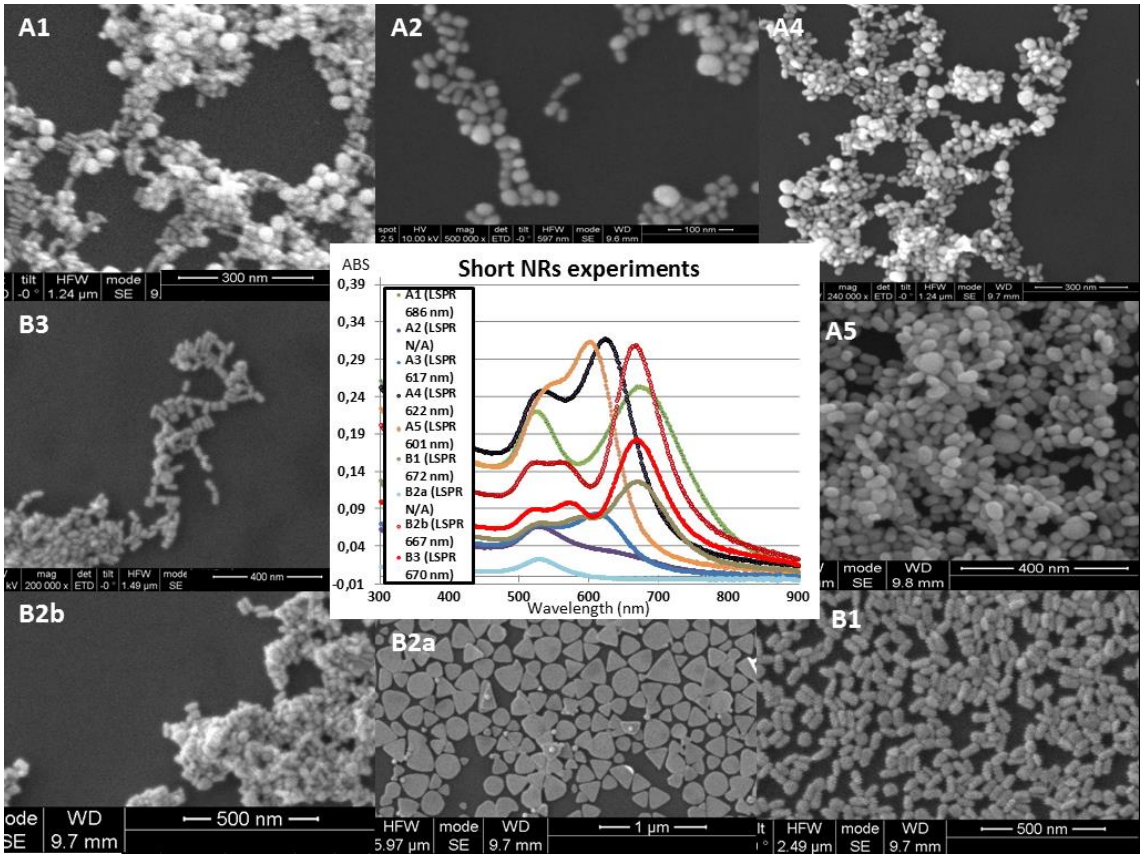

Figure 3.3 Overview of final UV-Vis spectra and SEM images collected from **NR-A** and **NR-B** experiments. Note that none of them was able to reach LSPR values far from 700 nm.

[39] Vigderman, L. & Zubarev, E. R. High-Yield Synthesis of Gold Nanorods with Longitudinal SPR Peak Greater than 1200 nm Using Hydroquinone as a Reducing Agent. *Chem. Mater.* **25,** 1450–1457 (2013).

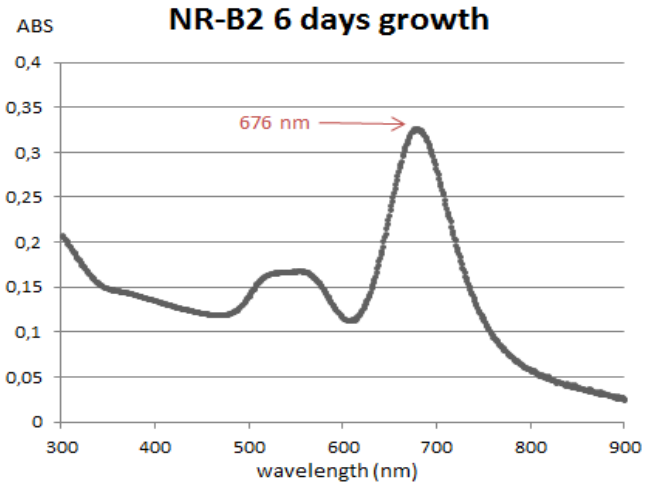

(left) Figure 3.4 Showing UV-Vis of NR-B2 experiment after 6 days growth immediately after it was derived to **B2a** and **B2b** experiments.

(down) Figure 3.5 a) **NR-B3** final UV-Vis spectra revealing both peaks from LSPR of NRs and SPR of pseudo-spheres. b) Histogram revealing the presence of the two described populations of nanoparticles. c) SEM and d) TEM images from **NR-B3** experiment that clearly confirm NSs presence.

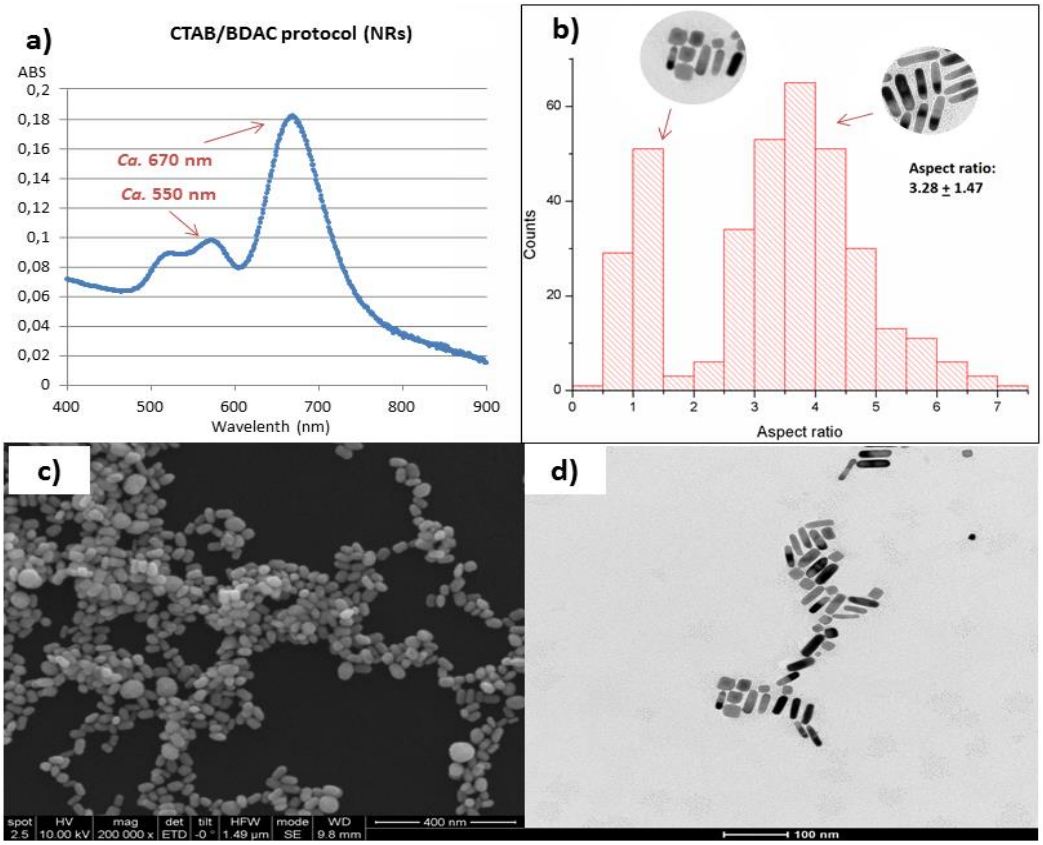

3.1.3 Synthesis of Gold Nanorods (NRs) with LSPR >1000 nm

The aforementioned unsuccessful attempts to reproduce the reported literature methods towards Au NRs with LSPR band at *ca.* 1064 nm, prompted one final search of the published literature. This search unearthed an article which obtained clearer evidence of the production of larger and/or slimmer NRs[39], and establish a synthetic procedure that covers and improves some of the drawbacks observed on previously performed experiments. As per the previously described NRs synthesis, it also follows the so-called "seeded-growth method". However, the authors' main

change in the procedure consists of the usage of hydroquinone as a reducing agent with lower reducing capacity, which allows a slow reduction of gold and leads to a more tunable and high yield NR synthesis, with an almost quantitative 100% gold conversion (that in this case is the limiting agent) compared with previously *ca.* 15% gold conversion to NRs, that also helps to avoid the formation of other structures as NSs observed in dual surfactant synthesis. It also allows working into a wider molar window compared with ascorbic acid, which was around 1.1 times Au(III) molar concentration, allowing to work with 10-20 times more concentrated reducing agent, that contributes to reduce the influence of weighting errors increasing reliability and reproducibility.

3.1.3.1 Standard protocol

All steps described by the protocol were followed to the letter[39], but as a result of our repeats, the following observations were made: In order to increase CTAB solubility and stability the CTAB stock solution (0.2 M) was sonicated at 40 ºC for several seconds until clear; all dilutions containing CTAB were kept at 37 ºC including during aging step; seed solutions did not revealed a "greenish" color as described in the method by Zubarev and co-workers; $NaBH_4$ addition was performed from a x200 times concentrated dilution in 1M NaOH, as it successfully produces *ca.* 3 nm seeds and avoid the influence of possible changes in Milli-Q water pH experienced in previous attempts; after several hours aging samples were washed from surfactant, as it was sufficient to reach 1000 nm LSPR, avoiding excessive enlargement of NRs and to avoid the crystallization of CTAB; and washing was performed by multi-step centrifugation-washing at 13000 rpm for 5 min until all excess surfactant was removed from suspension of colloidal particles. Furthermore, a PEGylation step was added after washing in order to substitute remaining CTAB attached to the NRs surface as an attempt to increase the colloidal stability and allowing nanoparticles to be conjugated with biomolecules required for subsequent studies.

Two experiments were performed following this method: **NR-C1** and **NR-C2**. First **C1** experiment was tested at room temperature, revealing LSPR higher than 1000 nm after several hours and crystallization of CTAB after overnight aging. Crystals were resuspended by sonication during a few seconds and washed several times at 13,000 rpm for 5 min at room temperature. We observed that during washing, almost all nanoparticles stuck to CTAB aggregates, preventing any washing and/or spoiling the sample. No NRs could be purified from **NR-C1** mainly for that reason.

To avoid this last drawback of the method, **NR-C2** was performed with the following changes: first centrifugation step was performed at 37 ºC to avoid the precipitation of CTAB; all of the subsequent washing steps were performed as usual. Aging was stopped after three hours, as

plasmon wavelength reached 1044 nm, and subsequently washed at 37 ºC followed by UV-Vis performance, revealing a slight wavelength shifting (1011 nm LSPR). The sample was stored undisturbed at room temperature overnight and UV-Vis was then performed again to test sample stability revealing a plasmon of *ca.* 995 nm, probably because an improperly performed washing of the bulk material. One last washing step was performed, obtaining a plasmon at 983 nm. **NR-C2** sample was monitored for several days and considered stable, as no more shifting on LSPR was detected after the fourth washing step. All previous blue-shifts detected by UV-Vis spectra were considered by changes at aspect ratio of NRs as described by several authors[9,11,38,39] caused by centrifugation steps and by partially washed reagents. However, dramatically changed LSPR absorbance values require further studies in order to discard possible inhomogeneous mixing, increased yield of post-washed sample **C2** during night, increased thickness of NRs overnight and/or a dramatic change of Ɛ value influenced by change on the aspect ratio that would cause huge variations in LSPR absorbance. If demonstrated, it would be crucial to keep same aspect ratio to allow proper concentration estimation of samples.

Track exp	LSPR (nm)	Variations
St1	1020	Standard protocol
St2	1024	Standard protocol (duplicate)
Seedx2	1038	Two times more seed sol.
Seedx3	1013	Three times more seed sol.
Ag35	1014	Half amount of $AgNO_3$
Ag105	1098	Double amount of $AgNO_3$
HQ25	900	2,5 times more hydroquinone
HQ50	795	5 Time more hydroquinone

Table 3.2 and Figure 3.6 respectively show the experimental conditions and the measurements obtained for reaction **NR-C3**.

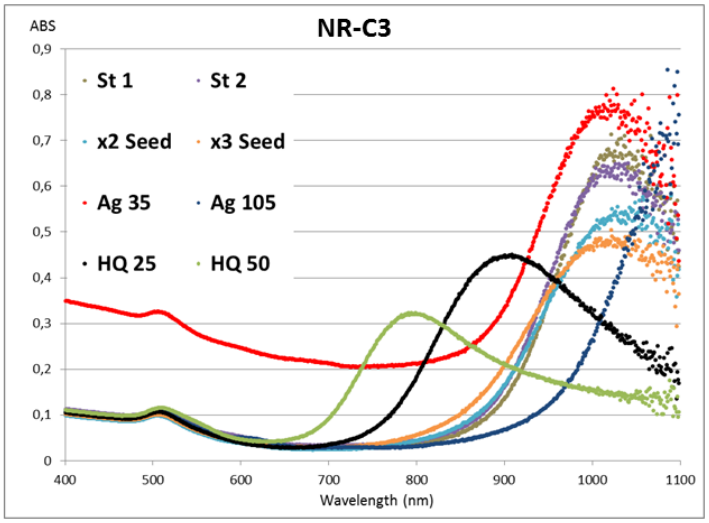

Once the synthetic procedure is well established and seemed viable, several experiments were performed by varying most of the key points of the protocol as an attempt to reach as higher LSPR values as possible. These experiments, labelled **NR-C3**, and consists of the comparison between UV-Vis spectra collected during the growth process of: two separate standard protocols (plasmon peaks at 987 and 977 nm), and the comparison with the addition of ½ the amount of $AgNO_3$ required (977 nm), a x1.5 times increased $AgNO_3$ volume (1070 nm), x2 and x3 seed volumes (990 and 987 nm respectively) and x2.5 and x5 times more volume of hydroquinone (863 and 766 nm respectively). The LSPR values obtained during the process are shown in Table 3.2 and depicted in Figure 3.6. Considering the inevitable variations observed between various repetitions of the same synthetic protocol, virtually all results obtained from these studies correlate with the described conclusions of the literature[39]. The inescapable conclusion is

that, although there are methods that give us the opportunity to produce NRs at higher aspect ratios and consequently an apparently more appropriate LSPR band (as it is the case of the decreased amount of $AgNO_3$ sample) the conditions revealing the optimum NR production were those coming from standard protocol, that was the chosen procedure for future synthetic performances.

PEGylation steps were crucial to obtain high stable bio-compatible nanoparticles. The conjugation of SH-PEG-COOH to the gold surface by its thiol group was performed immediately after the last centrifugation steps. Experiments performed this way demonstrate that NRs are properly stabilized by using a similar stabilization protocol as the protocol used for NNs synthesis. Two different lengths of PEG were studied: 3 kDa and 5 kDa SH-PEG-COOH. As the average surface value of these NRs is yet known and difficult to determine[8,9,11,14,37,39], the protocol was established in the first place to expose NRs to a large excess of polymer to properly cover as much of the NRs surface as possible. Amounts of PEG were calculated by considering 100% gold conversion to ensure this excess. Both stabilization procedures were performed simultaneously from a uniformed mixed double synthesis, in order to avoid any possible variation between protocol performances. Samples were monitored by UV-Vis spectroscopy, revealing LSPR values of *ca.* 980 nm for 3 kDa stabilization process and *ca*. 990 nm corresponding to 5kDa PEGylation. The colloidal stability was tested 24h before the last stabilization step was performed in order to allow formation of any possible aggregated form. It was tested by filtering both volumes using a 0.22 μm sterilization filter, revealing a lack colloidal stability of 3kDa-conjugated NRs as they get packed and aggregated on the top of the filter, while 5kDa stabilization protocol successfully passes almost the entire amount of gold NRs through it. These results are quite interesting as 3 kDa PEG seemed to fail to successfully stabilize gold nanorods, while an increased polymer tail (5 kDa) makes stable and well-defined clear NR solutions without a great impact in LSPR values.

Finally, as it is established by the literature, the number of washing steps prior stabilization is crucial as fewer steps would not properly wash the high amount of CTAB required for synthesis of NRs. Adding more washing steps than the optimum would entail lower aspect ratios together with high NR loss during the process. To test this, three experiments (labeled **NR-C4**) were performed using one, two or three 13000 rpm 5 minutes centrifugation steps at 37 ºC followed by PEG stabilization. The experiments were monitored by UV-Vis spectroscopy (Figure 3.7). The results revealed that although one single washing step prevents a large amount of NR loss, two washing steps gave more stable NRs with LSPR band at 1007 nm compared with 970 nm of one single washing step method. Three washing steps lead to a huge NR loss during purification, giving a similar LSPR band as shown for two-steps wash. The presence of CTAB is clearly seen on the <300 nm region of spectra, were most pollutants, non-reacted compounds

and/or by products absorb. SEM images were taken from the three of the samples (Figure 3.7), revealing large amounts of CTAB present in the single-step washing sample together with extremely low aspect ratio NRs, probably produced during sample desiccation[9,39] , showing evidences of a lack of stability of the sample. Two-steps washing sample on SEM revealed small amounts of CTAB, which presence dramatically decreased in the three-steps washing sample. NRs showed stable enough configurations on both samples. It was clearly seen that one single washing step did not totally remove most of CTAB dissolved, as opposed to 2 and 3 washing steps that lead to a similar level of purity of NRs as most of the CTAB peak has disappeared. Two washing steps are sufficient to clear almost all CTAB dissolved, allowing PEG to properly stabilize gold NRs.

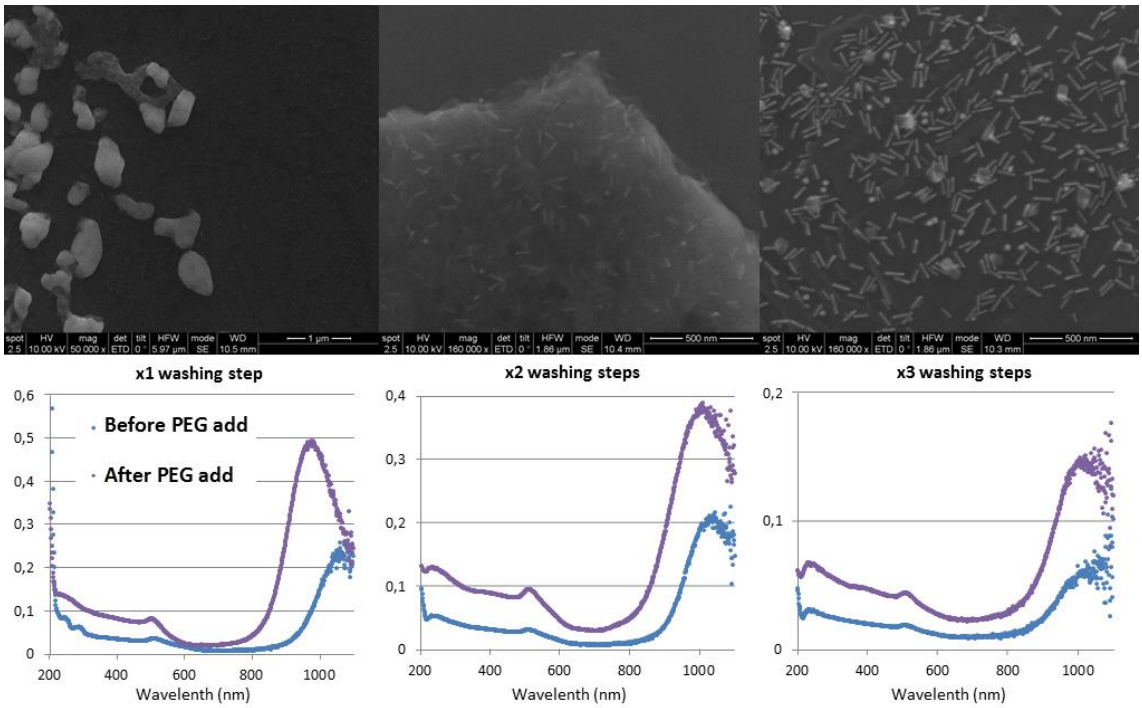

Figure 3.7 Representation of UV-Vis spectra for each experiment to test the number of optimum washing steps with their respective SEM images. Blue: before PEG addition, blue: before PEG addition, purple: after PEG. Samples were concentrated at the last step of PEGylation.

3.1.3.2 Optimized scaled-up protocol

The previously described protocol follows the low-scale procedure described on the literature, and successfully produces long aspect ratio NRs with LSPR higher than 1000 nm. However, it is mandatory to improve several aspects of the synthesis of NRs, to allow obtaining practical volumes of nanoparticles, minimizing any change in the optical properties, and adding some steps to increase the concentration of the final solution to make it practical for *in vitro* cell studies. Resulting samples were monitored by SEM, TEM and UV-Vis spectroscopy (Figure 3.8) and histograms were obtained that revealed an aspect ratio of 6.59$\pm$1.59.

This way a scaled-up protocol was developed by optimizing several key points of the synthetic procedure established in the literature by modifying and/or changing some of the steps seen in the previously described standard protocol. The total volume of the sample was increased by one order of magnitude, potentially allowing the synthesis of 10 times more quantity of nanoparticles, which should be sufficient for the subsequent applied research in cells. This means that although seed solution should be performed the same way as for standard protocol, adding to the growth solution 10 times more volume as before, the homogeneous exposure of the bulk material to the reducing agent before seed addition is crucial in order to obtain the maximum homogeneity of starting growth material as variations on the reduction levels of gold in the sample would potentially yield to a more inhomogeneous growing process[9, 14]. To better reduce the homogenization time while adding hydroquinone to the solution, stock concentration was increased by five times higher than required, allowing for the possibility to decrease the volume from five to one single millilitre that is easier to manipulate and quicker to add to the 100 mL volume.

Centrifugation and washing steps are another issue. The best value that we have at our disposal to scale up centrifuge conditions into larger volumes is "G" (with a calculated value of 15000G in previously described standard protocols). However, due to intrinsic centrifuge characteristics, samples are not able to form well-defined pellets on the bottom of bigger centrifuge tubes at such G and time conditions. Following the statement that increasing centrifugation strength may lead samples to undergo non-desirable blue shift on their longitudinal plasmonic wavelengths, the only way to carry out a well performed washing step was to increase centrifugation times from 5 minutes in the original protocol to 15 minutes.

Time consumption is also a key point at these steps as the longer the process takes place, the higher the chances of NRs to aggregate one to each other are, resulting in a high NR loss and decreasing the final aspect ratio of the nanoparticles. For this reason, an optimized washing-stabilization protocol was performed by adding two partial PEG stabilizations between each of the last centrifugation steps. Another remarkable change from standard to optimized protocol is that while performing washing steps, it was mandatory to reduce volumes in order to make samples easier to work with, and also to increase the exposure of NRs to the PEG solutions while sonication takes place, reducing the chances of producing aggregated forms.

Although this may affect the final CTAB concentration after wash, it is important to highlight that the key step in which most CTAB is removed belongs to the beginning of the washing process, immediately before first PEG stabilization step takes place. Surfactants on the surface of NRs are into a dynamic equilibrium with the media, attached by non-covalent mostly

hydrophobic interactions[7,40]. By removing as much supernatant as possible at these steps it is possible to change that dynamic balance on our favor, decreasing the amount of CTAB on NR surface that helps PEG to successfully reach gold surface and form a conjugated stronger bond thanks to its thiol groups, keeping NR stable in a CTAB-depleted medium.

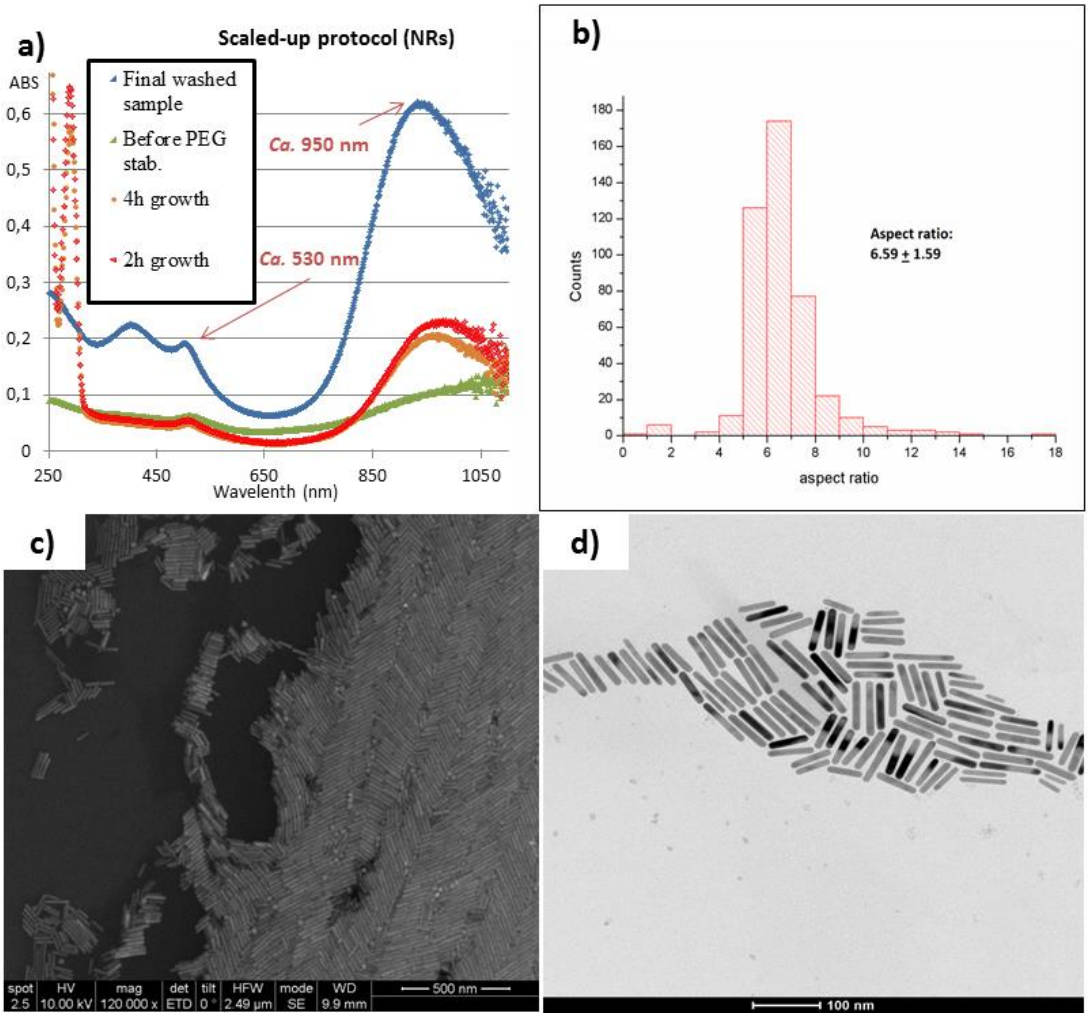

Figure 3.8 a) Representation of the progressive Uv-Vis spectra all along the synthesis process; b) Histogram of optimized scaled-up protocol revealing almost no NSs presence; c) SEM and d) TEM images of long NRs.

3.1.4 Functionalization of gold nanoparticles (NRs, NNs)

A standardized functionalization protocol was performed for both NNs and NRs[41]. This consisted firstly on the activation of the carboxylic groups on the exposed end of PEG molecule by the addition of pre-activated carbodiimide EDC and sulfo-NHS that may be used to form active ester functionalities with the carboxylate groups. Hydrophobic NHS esters couple with amines on desired molecules, giving them the nucleophilic power to attack the carbonyl group

[40] Moros M, Hernaez B, Garet E, Dias J.T, Saez B, Grazu V, Gonzalez-Fernandez A, Alonso C, and de la Fuente J.M. Monosaccharides versus PEG-Functionalized NPs: Influence in the Cellular Uptake. *ACS nano* 2012 **6** 2 1565–1577.

[41] Hermanson, G. T. *Bioconjugate Techniques*. – 2nd Edition

of the ester, releasing the sulfo-NHS group and creating this way an amide bond with the amine group. The final product of this two-step reaction is stable amide linkage. Figure 3.9.

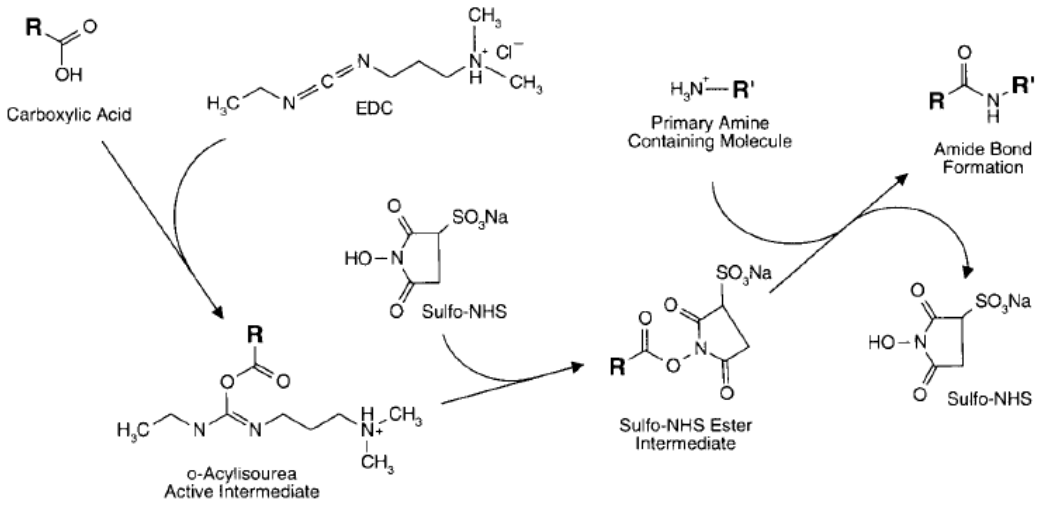

Figure 3.9 Depicted the chemical process carried out during amide bond formation. The efficiency of an EDC-mediated reaction may be increased through the formation of a sulfo-NHS ester intermediate. The sulfo-NHS ester is more effective at reacting with amine-containing molecules; figure from reference [41]

To increase the efficiency of the reaction, the concentration of added sulfo-NHS has to be much greater than the concentration of target carboxylic groups, which have to be at high concentrations to ensure a properly performed reaction. Both EDC and S-NHS were added at empirically optimized proportions, followed by the loading of samples into a Sephadex® column to remove the excess of reagents. During the period of time by which the carboxylic groups are activated, usually from 30 to 60 minutes[41], TAMRA and/or 4-aminophenyl β-D-glucopyranoside (generically referred as glucose) are added at the optimum proportions (empirically determined) in order to ensure the covalent bond formation. It is important to protect the sample from light sources to avoid photobleaching of the fluorophores. The reaction takes several hours to be almost complete[41]. To ensure an optimum efficiency all functionalizations were incubated overnight and the resultant solution was loaded again into a Sephadex® column to remove unreacted compounds, producing fully functionalized glucose or glucose/TAMRA nanoparticles.

During the whole process, Sephadex® columns and nanoparticles are equilibrated, resuspended and eluted in presence of 25 mM MES buffer to avoid any undesired pH fluctuation during the functionalization. A commercial modified glucose was used on these studies with an amino-phenyl group that stabilizes the amide bond formed during functionalization of the nanoparticles, and it also serves as spacer to avoid any other undesired interaction with the rest

of the molecule. Amine groups from both amino-phenyl-glucose and TAMRA react with the carboxylic acid forming an amide bond.

Gold calculation for NRs was considered by two ways: first studies considered 100% of conversion of the amount of gold salt into NRs as determined elsewhere[39]. However, in our studies there were evidences of a relatively high NR loss during the whole process of synthesis, washing, stabilization and activation of carboxylic groups, and a rough estimation of the amount of gold present in the resultant solution was obtained by cryodesiccation and weighting of resultant pellet into a high precision micro balance. This way it was possible to obtain a rough constant correlation between the LSPR absorbance value of the peak and the amount of gold present in the sample, with a value of ε=13.9 mL mg^{-1} cm^{-1} that could be used the same way as for NNs. The aforementioned difficulty in determining NRs gold surface makes it difficult to estimate the quantity of free carboxylic groups available for the functionalization, and NRs functionalization was followed as close as possible to the protocol performed in the case of NNs as it was already demonstrated to work on several other gold crystal structures[13, 19].

Two different functionalizations were performed in these studies for each of the two nanoparticles: Glucose single-conjugated and glucose/TAMRA dual functionalized nanoparticles. The former was used for irradiation experiments and the second was prepared for microscopy imaging and studies of internalization. Both were stored at 4 ºC light-protected and were prepared within a maximum period of one week prior use to prevent from any possible change in their properties. Both types of functionalized nanoparticles were characterized by UV-Vis spectroscopy and SEM imaging for both NNs and NRs, showing no relevant dissimilarities.

3.2 Measurement of the heating capability

Two different procedures were used with the aim of studying the heating capability of the brand new NRs and their homogeneity, to clearly see whether the nanoparticles used for the following cell-lines studies were stable enough under specific experimental conditions, and to lay the foundations for future studies to compare the efficiency of different anisotropic conformations of gold nanoparticles on converting light energy into heat.

Laser was adjusted to the bottom area of 96 wells plates that were selected for both experiments. Although the laser emission behavior corresponds to a homogeneous non-dispersed and fully collimated beam that only covers the totality of the bottom area of one single well on each irradiation, any possible digression of any kind while the beam makes contact with the plastic material of the plate should be avoided to the extent possible. It should be noted that under laser

irradiation the temperatures reached on the surface of the Au NP samples should be much higher than the bulk. Since laser was configured to function at maximum power (for the working laser configuration; see "*5.1.2. Experimental details"*), it is also important to avoid heat produced during the irradiation to spread through the plate raising the temperature of adjacent wells that may affect following measurements. To avoid pre-heating adjacent samples by both diffraction of the beam and/or by heat diffusion, two empty wells were located in between samples, as an attempt to minimize any heating of non-irradiated samples prior its measurement.

Nanoparticles polar solvents (water and/or culture media) were used as blanks, as it is described on the literature that there is no significant variations between heating capability of gold NSs (SPR = 520 nm) and the intrinsic heating produced by buffers[36]. Samples were firstly adjusted at two times concentration in Milli-Q water and then diluted 1:1 in the equivalent volume of DMEM as an attempt to minimize the influence derived from variable medium proportions, thus using a 1:1 Milli-Q-DMEM dilution as blank. All irradiations were performed at working laser configuration (100%). Samples were prepared and measured in triplicates.

3.2.1 Heating trial I 'HT-I'

Although it is theoretically and empirically established that nanomaterials with a LSPR band at the NIR region are capable to convert the incident light into heat, it is mandatory to probe and define whether the products obtained from the synthetic methods described previously are capable to induce heat and the extent to this conversion. Moreover, the comparison of the capability of producing heat between different gold shapes at the nanoscale is of crucial importance.

Three repetitions of optimized scaled-up protocol were studied, named **NR-D1**, **D2** and **D3** respectively, and a fourth one was performed by adding 5 times more reducing agent to the growth solution, resulting in a blue shift of the LSPR, allowing the sample to be used as negative control. Another batch of enhanced protocol of NNs was used as positive control. Their LSPR values obtained by UV-Vis spectroscopy were 935, 890 and 937 nm for each of **NR-D1**, **D2** and **D3** batches respectively, and *ca.* 1050 and 790 nm for positive control NN and negative control NR respectively. By using three different batches from the same synthetic protocol dissimilarities between repetitions and the influence of changes in the plasmon wavelengths of each one can be evaluated, as well as give some rough insights about possible variations on the heating capability of NNs and NRs with higher reliability. At the establishment of the conditions on this first experiment, the calculation of the amount of gold was not possible for the case of NRs. In order to make future molar calculations easier, all samples were diluted in Milli-Q water until ABS values at LSPR peaks were at an arbitrary value of 0.8 that was

considered the reference stock concentration. The results obtained from this first experiment are shown on Figure 3.10, where it is clearly revealed the heating capability of both NNs and NRs compared with diluted DMEM that was used as blank. It is also remarkable that under this experimental conditions it was not possible to see significant differences between any of the three batches of NRs, that displayed a Δt = 27 and 27.1 and 26.3 ºC respectively. Although there is a considerable high standard deviation between each of the triplicate reading of each batch, by calculating the average of all the three batches they displayed an almost null deviation (±0.35 ºC at most) that leads to suppose reproducibility of the synthetic protocol. The difference of light conversion into heat by NN was Δt = 19.8 ºC, which cannot be compared with NR measurements as molarity is not defined yet. There was also some expected over-heating at the blank (Δt = 6.8ºC) that correlates with the literature[36], probably produced by the proximity of water absorbance spectra[9]; and the negative control also showed a slight increase in temperature (Δt = 12ºC), that was not surprising keeping in mind that it revealed some remaining absorptivity at 1040 nm.

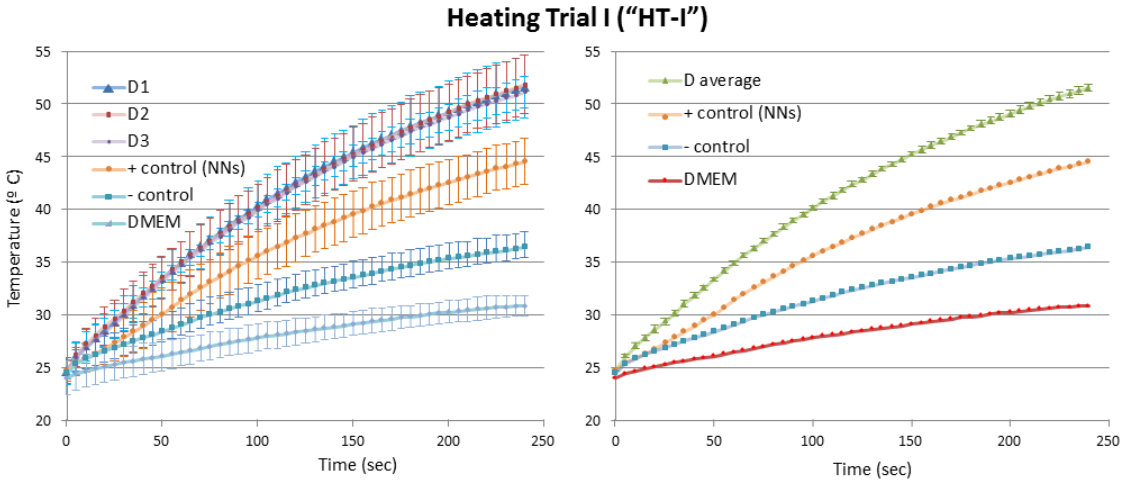

Figure 3.10 Left: heating ramps representing the three of the NR stocks with a positive control consisted of NNs at 0.2 mg/mL and a negative control of shorter NRs with blue-shifted LSPR. Right: Average of the three previously performed ramps with their standard deviation. Controls remained the same as before.

Slight changes between optical properties of gold nanoparticles are observed even between different experiments of the same protocol, revealing the importance of statistics to ensure enough homogeneity between different batches. However, the amount of gold is only practical to measure the effective number of particles if there is the same type and produced under very same conditions, thus correlating molar concentration to weight. To better study the heating conversion capability of each different type of nanoparticle it would be interesting to know the exact average amount of gold in each particle in order to obtain a molar value that helps equalizing the quantity of particles inside the sample. It is at this point that it is mandatory to

highlight the difficulty to obtain a reliable and effective molar value, as the difficulty to obtain an average of gold molecules per nanoparticle is directly dependent on the complexity of the synthetic procedure. This complexity may affect its homogeneity and subsequently its geometric adjustment, which is influenced by the packaging of the gold molecules that also depends on the presence of other possible soaked metals added during the synthesis (i.e. silver), homogeneous addition of reducing agent and/or seeds, the nature of the reducing agent itself, possible interactions with the vial containing the reaction, interactions of nanoparticles with each other or the behavior of the surfactant at different conditions of local concentration or temperature variations, among others. Although it would be interesting to compare equal molarity values, the inescapable conclusion is that even with slight blue-shifted non-regular LSPR values, laser-coupled heating remains very constant and precise, revealing a low deviation and responding equally to incident light, making the optimized scaled-up protocol valid for further studies. Finally, it must be acknowledged that these results correlate with recent reports in the literature[36].

3.2.1 Heating trial II 'HT-II'

After demonstrating the generation of heat by previous studies, and when all concentration calculations were properly established, a new heating trial was performed to test the heating capability of the nanoparticles in the context of cell culture conditions (37 ^{o}C/ 5% CO_2) to which samples will be exposed during cell studies, providing information about changes in their optical properties, conformation and/or stability by monitoring several parameters by UV-Vis and SEM imaging during the process.

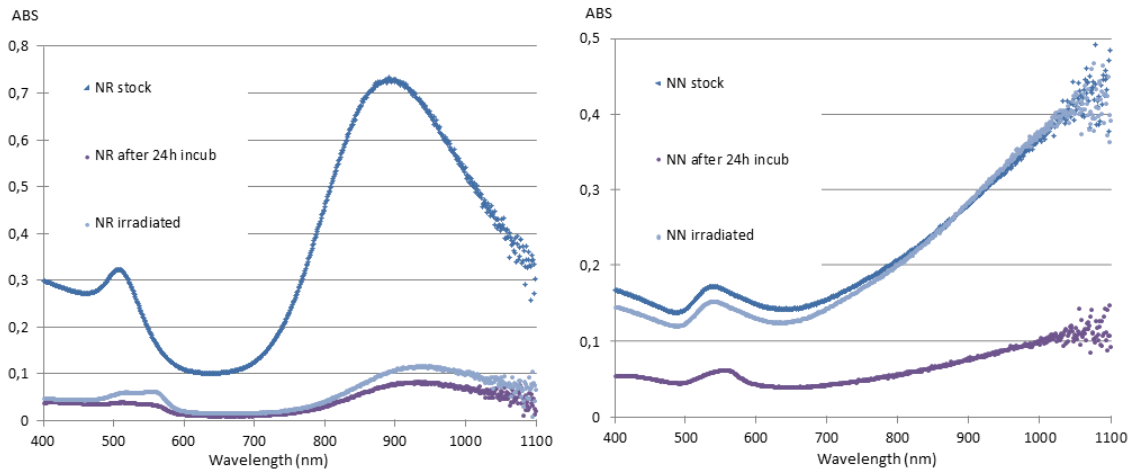

Figure 3.11 Monitoring of NR (left) and NN (right) all along the process of incubation and irradiation. Respectively: UV-Vis of stock solution, after 24h incubation in DMEM and after irradiation, blue, light blue and purple.

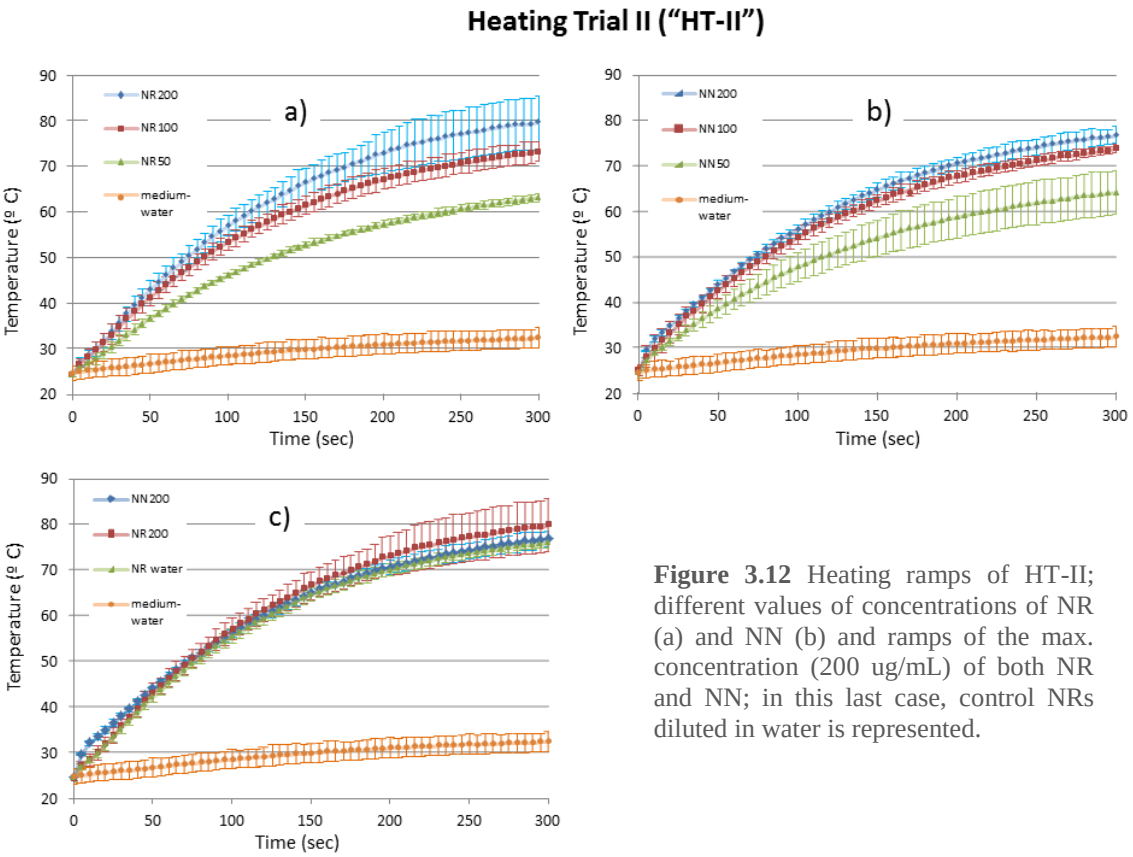

Figure 3.12 Heating ramps of HT-II; different values of concentrations of NR (a) and NN (b) and ramps of the max. concentration (200 ug/mL) of both NR and NN; in this last case, control NRs diluted in water is represented.

All NN and NR batches were the same as for HT-I. Based on previously revealed homogeneity, **NR-D1**, **D2** and **D3** batches were mixed together and treated equally. Concentrations were calculated as previously described (see *"3.1.4 Functionalization of gold nanoparticles"* for further information) and serial stock solutions of both NNs and NRs were prepared in Milli-Q water, and finally diluted 1:1 in DMEM. One extra control was added to the sample: one single dilution of 200 µg/mL NRs (a mixture of **NR-D** batches) diluted in Milli-Q water instead of medium. This sample was exposed to the same conditions and processes as DMEM-diluted nanoparticles, to check whether the medium affected the process. Samples were incubated for 24h under culture conditions to emulate the conditions to which nanoparticles are exposed during cell uptake. All samples were irradiated for 5 min and every step was monitored by UV-Vis (Figure 3.11).

The results revealed a non-linear proportion of increasing heating power with concentration. After 5 min exposure, NNs revealed a maximum temperature of Δt = 52.2, 48.7 and 39 ºC for each 200, 100 and 50 µg/mL concentration respectively. In the case of NRs measurements displayed Δt = 55.5, 49, and 39 ºC. Blank and control NRs revealed Δt = 7.77 and 51.4 ºC respectively, suggesting a properly performed assay. The highest standard deviations were observed at 200 µg/mL samples. Comparison of different nanoparticles at a single concentration value shows that heating capability of a specific concentration of nanoparticles is almost equal.

By now, it is clearly seen that both NRs and NNs have similar heating capabilities at a given weight concentration, thus it is possible to adjust cell dose in weight units (μg/mL). As standard, maximum studied concentration was selected (200 μg/mL) for all cell studies performed. Figure 3.12.

3.3 Studies of internalization of cells

Typically, endocytic processes for internalization of NPs (or other large-sized bodies) can be broadly classified in phagocytic and non-phagocytic mechanisms. First one occurs mainly in specialized cells and its function is protecting the organisms from exogenous elements or eliminating remaining structures derived from other physiological processes. Non-phagocitic pathways can occur in all cells and can be subcategorized into clathrin- and non-clathrin-dependent endocytosis; the last one can be further subdivided into three major mechanisms, *i.e.* macropinocytosis, caveolae-mediated endocytosis and clathrin- and caveolae independent endocytosis[40]. To date, pathways and rate of NPs uptake have been proven to be cell type dependent and furthermore, these vary also with NPs size, charge, funtionalization and other properties.

All protocols performed used 0.2 mg/mL of NNs or NRs synthesized respectively by the enhanced procedure or the optimized scaled-up protocol, which LSPR wavelengths were of 1080 and 970 nm, respectively. These AuNPs were functionalized with glucose for enhanced cellular uptake and TAMRA for a proper visualization by standard fluorescence microscopy. As it is not known how much TAMRA and glucose were attached to nanoparticles, these studies have just qualitative value, allowing studying the capability of functionalized nanoparticles to enter biological complex structures.

The cells selected for all these studies were Vero cells, a widely used well-known cell line isolated from kidney epithelial cells extracted from African green monkey (*Cercopithecus aethiops*). They were selected for their ease of use and well-established working protocols. Nanoparticles were sterilized with 0.22 μm filters followed by calculation of the concentration immediately before the inoculation of cells.

3.3.1 Standard fluorescence microscopy

Ibidi inoculation

Vero cells were cultured in μ-Dishes from Ibidi®, as this technology allows high level of cellular proliferation and aids with the adhesion of cells to their surface, as well as having a reference grid that helps on the location of plate areas. Samples were loaded into a culture

visualization chamber with temperature control to keep cell viability and as an attempt to avoid differences in cellular morphology to the extent possible. Samples were visualized by fluorescence and phase contrast microscopy on a Nikon Eclipse Ti microscope.

Fluorescence microscopy visualization

Phase contrast and standard bright-field microscopy, both combined with fluorescence were visualized and the presence of nanoparticles was studied. NNs-loaded samples revealed bright red fluorescence denoting the presence of nanoparticles. It is remarkable that even without any emission of fluorescence, NNs accumulate inside subcellular compartments at high concentrations that allowed their location even with bright field channel. As it was not possible to ensure that nanoparticles have entered inside cells or are, in turn, attached to outer cellular structures, confocal microscopy images are necessary. NRs-loaded samples, otherwise, did not revealed detectable fluorescence, probably because signal levels were too low, thus it was also mandatory to perform several visualizations under a confocal microscope.

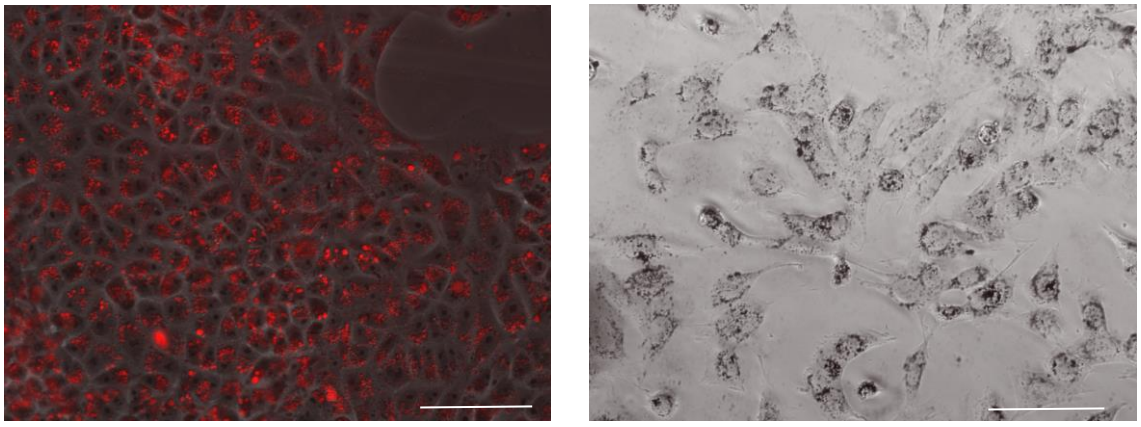

Figure 3.13 Left: Representation of overlapped bright field and red fluorescence corresponding to NNs. Right: Bright field representation, where it is possible to see the particles inside the vesicles even without fluorescence. All scales are at 100 µm

3.3.2 Confocal microscopy

Sample preparation and cells fixation

All samples were prepared and fixed duplicated. Prior to visualization using confocal microscopy, it is highly recommended to fix cells in order to preserve samples, and increase intensity of the fluorophores. It is also necessary to add an extra fluorophore (i.e. DAPI) to co-localize nanoparticles together with sub-cellular structures as the nucleus. Instead of standard PBS, it is mandatory to use DPBS (with extra Ca^{2+} and Mg^{2+}) in order to ensure cell integrity and a realistic fixation, avoiding alterations on cell morphology through such long and aggressive incubation times. Furthermore, it is also recommended to check cell morphology before each step during fixation by bright field microscopy. As this is the case, the use of

nanoparticles requires extra washing during the whole protocol. P-formaldehyde has a toxic and carcinogenic nature, that makes it highly recommended to work under the hood during the steps in which it is used.

Several samples were prepared with the following functionalizations: NNs functionalized with TAMRA (NN@Tamra) that were used to check if cells are able to internalize nanoparticles by alternative pathways apart from glucose-mediated pathways; NNs and NRs functionalized with glucose and TAMRA (NN@TamraGlc and NR@TamraGlc, respectively), the former served as positive control; and control sample with no nanoparticles (only DAPI) serving as negative and auto fluorescence reference.

Image collection

Samples were visualized using a Fluoview FV10i from Olympus®. All the images collected used the same intensity and hardware gain parameters for both lasers and no image treatment was applied afterwards, apart from 3D reconstruction. Control samples were visualized in the first place to check auto fluorescence and adjust the microscope until there is no background nor saturated pixels. With those parameters fixed, all the other measurements were performed (Figures 3.14, 15a and 15b).

Both NN@TamraGlc and NR@TamraGlc samples revealed the presence of red fluorescence inside cells. However, although it can be asserted with a high degree of certainty that cells are successfully internalizing both types of nanoparticles, it must be acknowledged that the distribution of fluorescence through the cellular volume is slightly different from each type of nanoparticle, as NNs seemed to be spread surrounding the nucleus while NRs were apparently more at the edge of the cytoplasm forming vesicles. This suggests slightly different internalization pathways for the two types of nanoparticles that may influence the effect of NIR irradiations. It has been previously reported that NPs modified with saccharides, once internalized in cells, are stored in endocytic vesicles[7, 8, 40] ; this seems to be the case here. As any other neither contrast nor marker was loaded to specifically locate other sub-cellular structures, further studies are required to explain these differences.

Images obtained from NN@Tamra revealed no red fluorescence, caused by the absence of NNs inside the sample. This way it could be asserted that under these specific assay conditions, glucose plays a key role in the internalization pathway of nanoparticles, and any alternative unspecific and/or glucose-independent internalization pathway can be discarded with a high degree of certainty. In fact, PEGylation itself should prevent the internalization of these NNs[40].

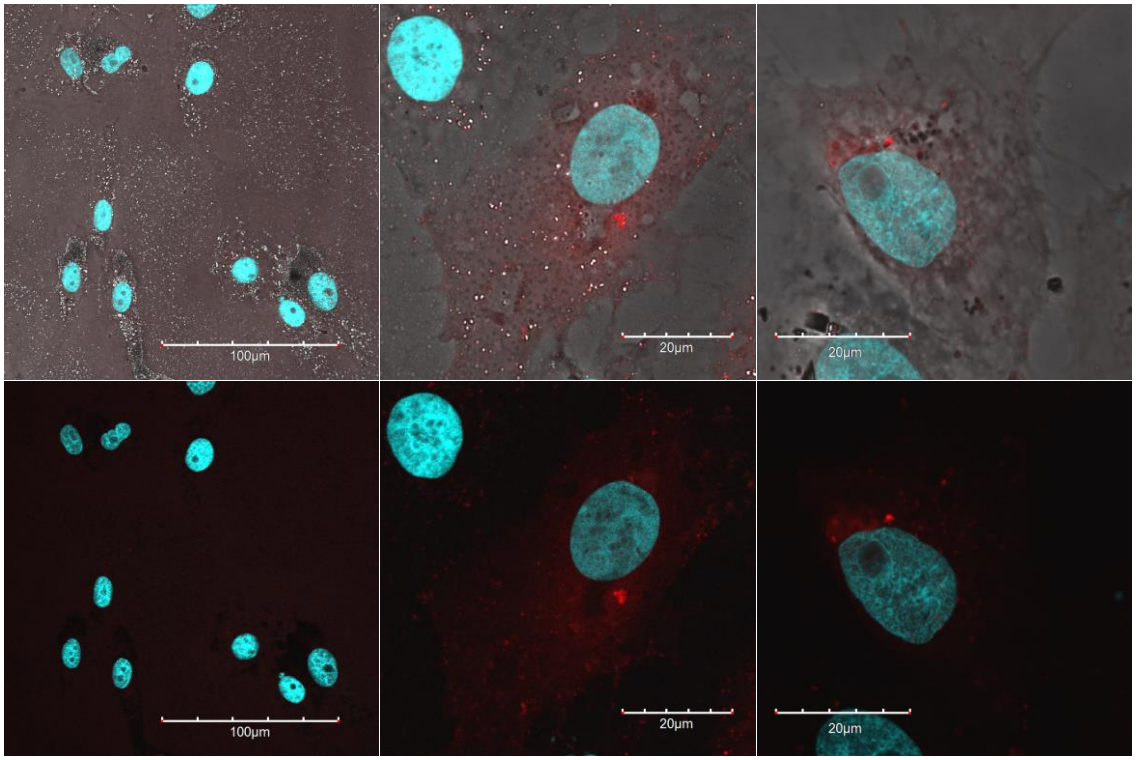

Figure 3.14 Up: all 3 merged channels; down: subtracted bright field. From left to right: Cells inoculated with NN@TAMRA; with NN@TAMRA&Glc; and with NR@TAMRA&Glc.

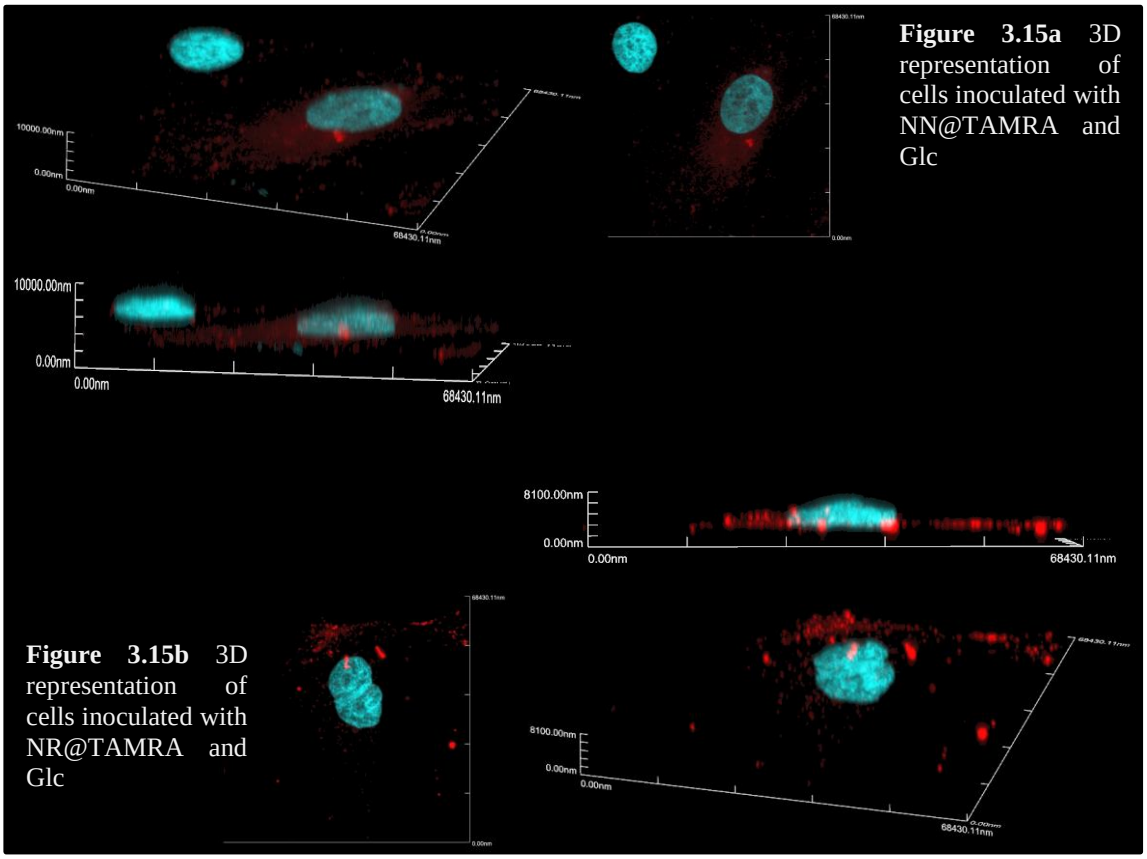

Figure 3.15a 3D representation of cells inoculated with NN@TAMRA and Glc

Figure 3.15b 3D representation of cells inoculated with NR@TAMRA and Glc

3.4. Using nanoparticles for optical hyperthermia using Class IV laser

3.4.1 Irradiation of Ibidi plates

Once demonstrated the optical characteristics of nanoparticles to derive light into heat at a considerable high efficiency and their capability to enter biological systems *in vitro*, the actual ability of these nanoparticles to induce cell death must be assessed. Several assays were performed, firstly as a proof of concept with NNs functionalized both with glucose and with glucose and TAMRA, and the behavior, rapidity of the apparition of cell death, and changes in morphology were evaluated (Figure 3.16).

Cells were cultured in μ-Dishes from Ibidi®, prior being inoculated with two types of nanoparticles: NN functionalized glucose and TAMRA (NN@GlcTAM), and NN functionalized with glucose (NN@Glc) to study any possible variation derived from TAMRA during irradiation. Once samples were irradiated under working laser configuration, they were loaded into a culture visualization chamber with temperature control to keep cell viability and as an attempt to avoid differences in cellular morphology to the extent possible. Samples were visualized by fluorescence and phase contrast microscopy on a Nikon Eclipse Ti microscope.

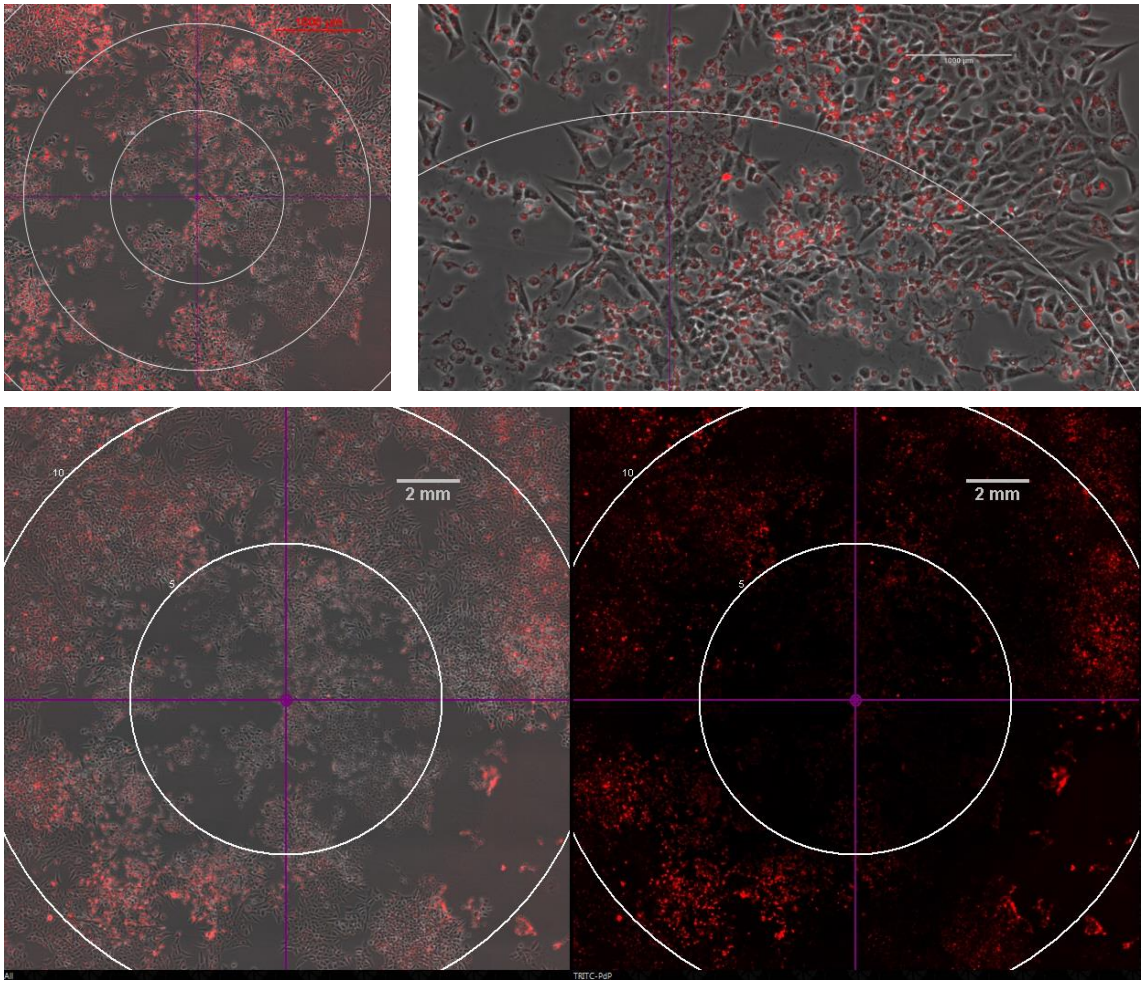

Figure 3.16 Upper left: Overview of the culture area before irradiation. Bottom: 2 channel (left) and single red channel (right) of irradiated area after several minutes. Upper right: detail of the limits of the irradiated area.

Images derived from irradiation clearly revealed an immediate cell death after 5 min irradiation. Cells started dying as a result of the presence of nanoparticles, as it could be easily seen that non-irradiated cells and/or cells that reveal low levels of red fluorescence keep the same morphology after a certain period of time (after 3h). Irradiated area was clearly defined as a result of changes on cell morphology and also as a result of diminished red fluorescence, probably derived from the release of nanoparticles to the medium after membrane disruption, whereas cells in the non-illuminated regions kept their fluorescence. While dying, cells started to form outer vesicles, nucleus start to change in conformation and cytoplasm start to acquire a spherical shape as a result from cell detachment from the plate. From the depicted cell morphology and the early apparition of changes all over irradiated area it could be assessed that cell death is most probably derived from a necrotic process rather than apoptosis. The same study was performed using NN@Glc as control and NR@Glc to compare the killing capability of nanorods. However, although NNs were totally capable for this purpose, NRs did not reveal any sign of changes on cell morphology. There are several reasons that could explain this unexpected result that will be discussed later (see *4. Conclusions and Future research*).

3.4.2 Vero assay LIVE/DEAD Assay - NRs vs NNs

In order to assess the cell viability of cells loaded with NN@Glc and NR@Glc, both laser irradiated or non irradiated, the live/dead® viability/cytotoxicity assay from Invitrogen® was used in selected samples; this test provides a two-color fluorescence cell viability assay that is based on the simultaneous determination of live and dead cells with two probes: calcein AM and ethidium homodimer (EthD-1), that measure recognized parameters of cell viability, as intracellular esterase activity and plasma membrane integrity, respectively. This way, this test provides a two-color fluorescence cell viability assay allowing to simultaneously determining live (green staining in the cytosol) and dead cells (red staining in the nuclei).

In NN@Glc sample, merged image of red and green fluorescence channels shows that the viability of irradiated cells was impaired, as red fluorescence was clearly seen all over the irradiated region. However, there was also some ambiguous staining, as some cases revealed both red and green fluorescence while other cells were not stained at all. These results clearly determine the capability of inducing cell death by functionalized NNs, and are in stark contrast with the observations of irradiation of cells that were inoculated with NR@glc, which were apparently unable to induce any effect on cell viability at these assay conditions. This lower capability could be derived from dissimilar internalization pathways and/or sub-cellular locations between NRs and NNs, the change in the heating capability due to changes in the optical properties once entered their destination organelle (*i.e.* derived from lower pH of

lysosomes) or by a possible but not probable capability of cells to eject NRs before being able to induce heat. Figures 3.17 and 3.18.

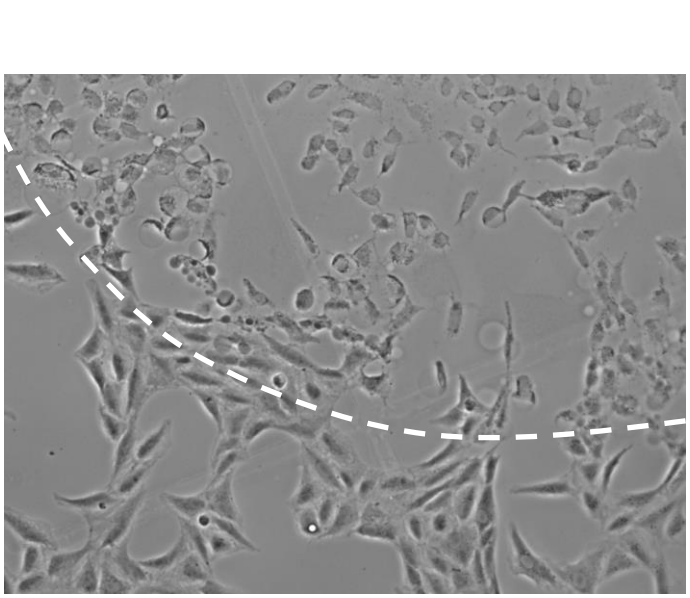

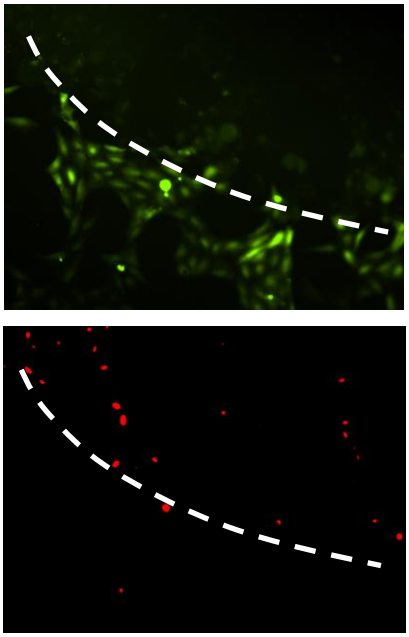

Figure 3.17 Detail of the irradiated area of cells inoculated with NNs. Right: green and red fluorophores of live and dead cells, respectively.

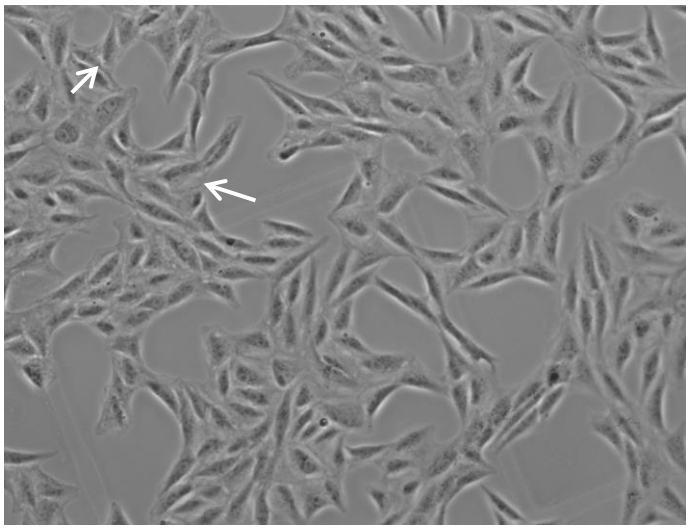

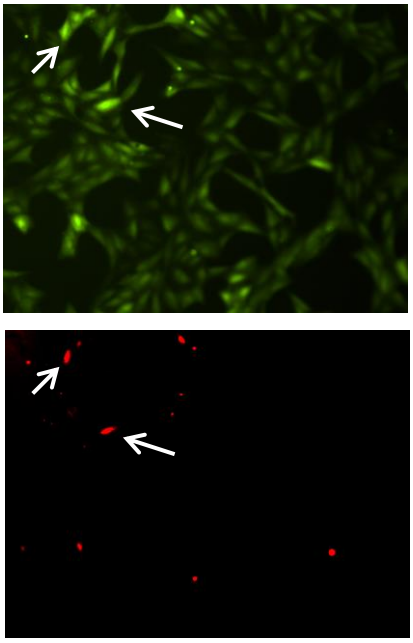

Figure 3.18 Region of the irradiated area after inoculation with NRs. Green/red channels revealed no lethal effect of NRs. Note there are some highlighted ambiguous staining.

4. CONCLUSIONS AND FUTURE RESEARCH

After arduous and sometimes futile research, anisotropic gold nanostructures were successfully obtained in high yield and with LSPR bands in the NIR region, centred as close to 1064 nm as possible (within the optical biological window), a wavelength that could be stimulated by Class IV 1064 nm laser to produce heat. Both obtained nanostructures, gold nanonachos (AuNNs) and nanorods (AuNRs), were successfully functionalized with sugars and fluorescent dyes to stimulate cell uptake and to identify their location inside cells, respectively. Furthermore, heating assays demonstrated the ability of both types of colloidal nanoparticles to produce heat and allowed for preliminary evaluation of the heating ability of each type of nanoparticle.

A straightforward method of producing AuNNs in water at room temperature without the use of highly toxic reagents has been described. The edge length and wavelength of the LSPR band can be tuned along the NIR range by adjusting the concentration/molar ratio of gold salt and reducing agent. A reliable and reproducible synthetic route towards AuNRs has been identified and optimized using a seed-mediated growth process involving CTAB. Importantly, the highly toxic surfactant CTAB can be replaced with PEG facilitating the use of these particles for bioapplications.

The presence of PEG polymer allows the surfaces of these particles to be functionalized with glucose for cell uptake and the fluorescent dye TAMRA to verify their internalization and locate the particles inside cells.

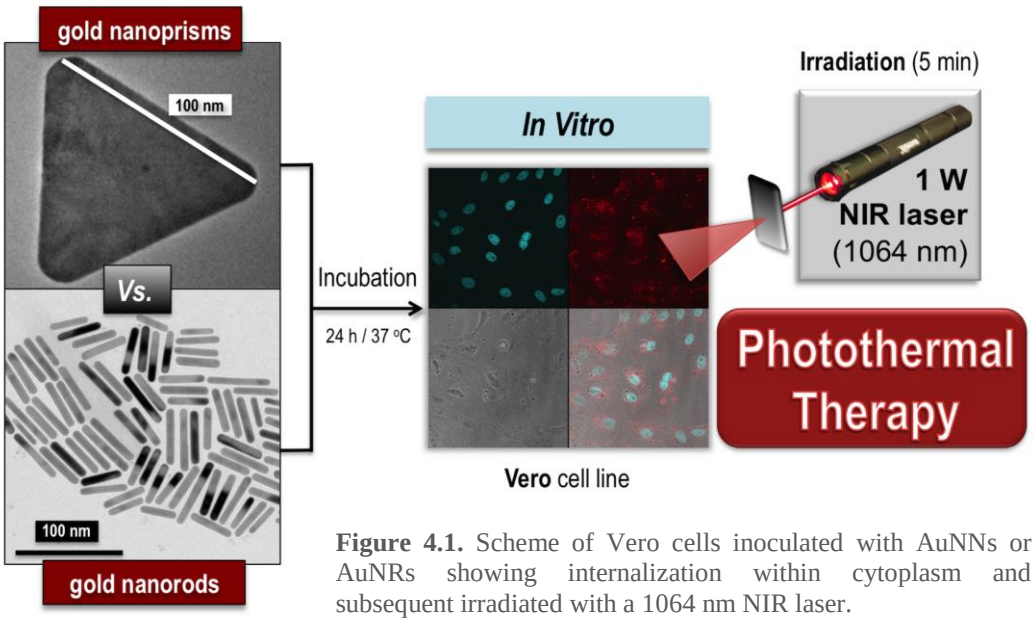

Figure 4.1. Scheme of Vero cells inoculated with AuNNs or AuNRs showing internalization within cytoplasm and subsequent irradiated with a 1064 nm NIR laser.

The use of both AuNNs and AuNRs as nanoheaters under NIR illumination (Class IV laser 1064 nm) was tested in aqueous solution and in cell media. Both types of colloidal gold nanoparticles were shown to be highly efficient heaters (*ca.* Δt = 50-55 ºC at a concentration of 02 mg/mL). Furthermore our studies showed that both the biofunctionalized AuNNs and AuNRs were stable in cell media.

Vero cells were incubated with AuNNs@Glc&TAMRA and AuNRs@Glc&TAMRA for one hour at 37 ^{o}C. Optical and confocal microscopy data verified the presence of large quantities of these NPs inside cells. Vero cells incubated with these AuNPs were irradiated with 1064 nm laser light for 5 min. In these preliminary studies the AuNNs were shown to be highly efficient at killing Vero cells upon NIR laser irradiation, whereas the AuNRs proved less effective. This lower capability could be derived from dissimilar internalization pathways and/or sub-cellular locations between NRs and NNs, the change in the heating capability due to changes in the optical properties once entered their destination organelle (*i.e.* derived from lower pH of lysosomes) or by a possible but not probable capability of cells to eject NRs before being able to induce heat.

As a result, a number of critical studies will be required in the future. Firstly, although TAMRA helps to identify the presence of AuNPs inside cells, the exact quantity of AuNPs present inside and their exact location is not known. The quantity can be determined by ICP elemental analysis of cells incubated with AuNPs and the exact location of the AuNPs can be identified using Transmission Electron Microscopy of fixed cells containing each type of AuNP. Further, a detailed cytotoxicity study involving MTT assays and cytommetry would assist in identifying more accurately the bioavailability of these AuNPs. In addition, critical concentrations for cell death by laser irradiation could be identified using cytommetry and laser irradiation of specific concentrations of AuNPs.

5. EXPERIMENTAL SECTION

5.1 Synthesis and characterization of nanoparticles

5.1.1. Reagents

Hydrogen tetrachloroaurate (III) hydrate, Sodium borohydride powder, Sodium hydroxide, sodium thiosulfate (STS), Hexadecyltrimethylammonium bromide (CTAB), Benzyl-dimethylhexadecylammonium chloride (BDAC), 1-Ethyl-3-[3-dimethylaminopropyl] carbodiimide Hydrochloride (EDC), 4% p-formaldehyde, 4-aminophenyl β-D-glucopyranoside and Sodium borohydride powder were purchased from Sigma-Aldrich and used as received. Potassium Iodide (KI) and Silver nitrate were purchased from Panreac®. Hydroquinone was purchased from Alfa Aesar®. Ascorbic Acid was purchased from Sigma®. Complete Dulbeccos´s media (DMEM) and phosphate buffer saline (PBS) were purchased from Gibco®. DMEM was supplemented with glutamine, bovine serum and antibiotic complex prior usage on any cell culture. NHS (sulfo-NHS) was purchased from Thermo Fisher®. 2-(*N*-morpholino)ethanesulfonic acid (MES) was purchased from BioRad®. Sephadex® columns were purchased from GE Healthcare. Prior to use, all glassware was washed with aqua regia and rinsed thoroughly with Milli-Q water from Q-POD® system from Millipore. All nanoparticle suspensions were sterilized with 0.22 μm MilliPore® filters prior addition to cell cultures.

5.1.2. Experimental details

UV-Vis spectroscopy: UV-Vis spectra of compounds of all colloidal solutions were collected using a Cary 50 Probe® spectrophotometer from Varian.

Scanning Electron Microscopy (SEM): SEM images and energy dispersive x-ray spectroscopy (EDX) spectra were acquired using a field emission SEM Inspect F50 with an EDX system INCA PentaFETx3 (FEI Company, Eindhoven, The Netherlands) in an energy range between 0-30 keV.

Transmission Electron Microscopy (TEM): TEM images collected using a Cs-probe-corrected Titan (FEI) operated at 300 kV.

Laser: A 3 W Laser Quantum Ventus laser system (1064 nm) was equipped with a single-mode TE_{00} fiber which illuminates the sample with a power per unit of area of *ca.* 30 $W \times cm^{-2}$ at the sample position. Laser emission wavelength was at 1064 nm. Working configuration through all protocols described in this document was at 100% power, giving *ca.* 1000 mW at a distance of 1 cm from sample surface.

Optical Microscope: Nikon Eclipse Ti with FPS system connected to NIS-Elements Microscope Imaging Software.

Confocal Microscope: Olympus Fluoview FV10i all-in-one confocal microscope system equipped with 559 and 405 nm lasers and 570-670, 420-520 nm band-pass emission detectors.

5.1.3. Synthesis of Triangular Gold Nanoprisms (NNs)

5.1.3.1 "Standard protocol" - Triangular Gold Nanoprisms (NNs) with a localized surface plasmon resonance (LSPR) band at 900 nm.

120 mL of freshly prepared 0.5 mM $Na_2S_2O_3$ (aq) (STS) was added dropwise to 100 mL of 2 mM $HAuCl_4$ (aq) over a period of *ca.* 1 min. This solution was aged for 9 min undisturbed prior to a second addition of 35 mL of 0.5 mM STS. Apart from homogenization, any shaking or disturbance of the sample should be avoided (including during aging) and the addition of STS to any solution containing $HAuCl_4$ should be carried out gently. The final solution is kept undisturbed for 60 min until the synthesis is complete. UV-vis spectra revealed a strong absorbance peak at *ca.* 550 nm and *ca.* 900 nm. Subsequent electron microscopy analysis revealed these to correspond to pseudo-spherical polyhedral gold nanoparticles and triangular gold nanoprisms ('nanonachos', NN), respectively.

5.1.3.2 "Enhanced protocol" - NNs with LSPR band at 1050 nm.

Firstly, 60 µL of 0.1 M KI solution were mixed with 220 mL 0.5 mM STS. 110 mL of previously prepared dilution (KI + STS) was added dropwise to 200 mL of 2 mM (aq) $HAuCl_4$ over a period of ca. 30 sec and aged for 4 min undisturbed, prior to a subsequent addition of 110 mL of KI + STS dilution followed by another 4 min incubation. Finally, 70 mL of STS was added to the mixture. The final solution was kept undisturbed for 60 min until the synthesis is complete. UV-vis spectra revealed a strong absorbance peak at *ca.* 550 nm and >1000 nm. Subsequent electron microscopy analysis revealed these to correspond to pseudo-spherical polyhedral gold nanoparticles and triangular gols nanoprisms ('nanonachos', NN), respectively.

5.1.3.3 PEG stabilization and washing steps.

NNs plasmon peaks were measured by UV-Vis spectroscopy. Using half of this O.D. value and applying a conversion factor (Ɛ) 25 mL mg^{-1} cm^{-1} (standard for NNs), the required PEG amount was calculated. PEG was diluted in 1 mL Milli-Q and a determined volume of a 10 mg/mL stock solution of $NaBH_4$ was then added to reach 1:1 molar ratio of PEG:$NaBH_4$. Each 1 mL PEG- $NaBH_4$ solution was completely added to NNs, and adjusted to pH 12 with ca. 2 mL 2 M NaOH under mild mixing. Finally, the solution was sonicated for 1h at 60 ºC, and then

centrifugued at 4500 rpm for 15 min at room temperature to precipitate the NNs and separate them from excess PEG and unreacted starting materials. Pellets were aliquoted in eppendorf tubes and centrifuged three times at 6000 rpm for 9 min at room temperature before removing the supernatants and each time resuspending the nanoparticulates in Milli-Q water. These final samples were diluted to one quarter of their original volume and aliquoted in 50 mL centrifuge tubes to let them decant at room temperature for several weeks. After this time the larger, heavier NNs sedimented at the bottom of the centrifuge tubes and the upper layer of the solution containing the smaller, lighter polyhedral gold particles could be removed.

5.1.4. Synthesis of Rod-Shaped Gold Nanoparticles (NRs)

5.1.4.1 NRs with LSPR <850 nm (CTAB and CTAB/BDAC-based procedure Liang-Tang – El-Sayed[11, 38].

These particles were synthesized as per the reported procedure. A seed solution was prepared by mixing 5 mL 0.5 mM $HAuCl_4$ (aq) and 5 mL 0.2 M CTAB (aq), followed by the addition of 600 µL of freshly prepared 10 mM $NaBH_4$ (ice-cold solution), under rapid magnetic mixing for 2 min. For this method, the seed solution was left undisturbed for 1-2 hours prior to use. Growth solutions were performed using two different surfactant mixtures: single surfactant solution (CTAB) and dual surfactant mixture (BDAC/CTAB at molar ratio of 2.77).

For first trials, the single surfactant solution was used. 40 mL 0.2 M CTAB (aq) solution was mixed with 40 mL 1 mM $HAuCl_4$ (aq) together with an appropriate amount of 4 mM $AgNO_3$ (aq) and followed by the addition of 560 µL 78.8 mM ascorbic acid (aq) (AA). The mixture was rapidly mixed and instantly became colourless indicating the formation of Au(I) from Au(III). Finally, a determined volume of seed solution was added to the mixture. Seeded-growth solutions were aged overnight and monitored by UV-Vis spectroscopy and SEM imaging.

After those first approaches, and as a variation of this method, the two-surfactant (BDAC/CTAB) growth solution was used at a molar ratio of 2.77 as described in the literature[11, 38]. This solution was prepared by adding 0.8 g CTAB (aq) to 5 mL 0.15 M BDAC (aq) (final CTAB concentration: 0.415 M), and sonicated for 20 min at 40 ºC following literature indications. The solution was added to 200 µL of 4 mM $AgNO_3$ (aq) followed by the addition of 5 mL of 1 mM $HAuCl_4$ (aq). Finally, 70 µL of 78 mM AA (aq) were added under rapid mixing until the solution became colorless, initiating rod growth by the addition of 12 µL of the previously described seed solution. The growth process was continued over a period of several days during which it was monitored by UV-Vis spectroscopy. Samples were washed and the resultant solution was observed by SEM imaging.

5.1.4.2(I) NRs with LSPR >1000 nm (based on Zubarev method[39].

All stocks and solutions containing CTAB were kept at 37 ºC. To prepare the seed solution, a stock solution of 1 M $NaBH_4$ (aq) dissolved in 1 M NaOH (aq) was first prepared; as well as 10 mL 0.5 mM $HAuCl_4$ (aq) + 0.1 M CTAB (aq). Both solutions were prepared separately at 1 mM and 0.2 M concentration respectively; CTAB required a few seconds sonication at 40 ºC to fully dissolve into solution. Then, 4.6 µL of previously prepared $NaBH_4$/NaOH stock solution was added to $HAuCl_4$ + CTAB solution. This brownish mixture was allowed to stand for a few minutes before use.

For the preparation of the growth solution, 10 mL 0.5 mM $HAuCl_4$ + 0.1 M CTAB solution (both compounds prepared separately at 1 mM and 0.2 M concentration respectively; CTAB was sonicated a few seconds at 40 ºC) was added to 70 µL 0.1 M $AgNO_3$ (aq), followed by addition of 500 µL 0.1 M hydroquinone (diluted in water from a x5 times concentrated fresh-made stock solution), under stirring until the growth solution became clear. Finally, 160 µL of seed solution was added. Experiments were aged until the plasmon wavelength reached 1000 nm, usually within 3-5 hours.

The first centrifugation-washing step was carried out at 13000 rpm, 5 min, at 37 ºC. The pellets were resuspended in Milli-Q water and received another centrifugation at 13000 rpm, 5 min; but this time at room temperature. HS-PEG-COOH concentration was estimated considering 100 % Au conversion, applying same formula as for NNs. This way, 3.7 µL $NaBH_4$ 1 mg/mL in 1 M NaOH (aq) were added to 100 µL of 0.49 mg/mL PEG solution and the entire volume was added to five hours-aged growth solution. The former solution was adjusted until pH 12 with NaOH, followed by 60 min of sonication at 60 ºC. This solution was then centrifuged 13000 rpm for 10 min at room temperature and pellets were washed with Milli-Q water. The final resuspended NRs were stored in Milli-Q water at room temperature. LSPR apparition was monitored during the growth process by UV-Vis spectroscopy and final solution was observed by SEM and TEM imaging.

5.1.4.2(II) Optimized Scaled-up protocol >1000 nm NRs.

All stocks and solutions containing CTAB were kept at 37 ºC. Seed solution was prepared as described (see 5*.1.4.2(II)* for further details).

For the preparation of the growth solution, 100 mL 0.5 mM $HAuCl_4$ + 0.1 M CTAB solution (both compounds prepared separately at 1 mM and 0.2 M concentration respectively; CTAB was sonicated a few seconds at 40 ºC) was added to 700 µL $AgNO_3$ (0.1 M), followed by addition of 1000 µL 0.5 M hydroquinone under stirring until solution becomes clear. Finally,

1.6 mL seed solution was added. Experiments were aged until the plasmon wavelength reached 1000 nm, usually within 5 hours.

For the scaled-up protocol, washing and stabilization were performed simultaneously. Firstly, 9.85 mg PEG diluted in 2 mL Milli-Q water were added to 74 µL of a freshly made 1 mg/mL NaBH4 and left undisturbed for three hours, ice-cold. The entire volume was divided in two and added to 100 mL and 50 mL 37 ºC pre-heated Milli-Q water respectively. Growth solution was centrifuged at 13000 rpm, 5 min, 30 ºC, and pellets were resuspended in 37 ºC pre-heated Milli-Q water. A second centrifugation step was then performed, followed by resuspension of pellets with previously prepared 100 mL pre-heated PEG dilution. The resultant solution was adjusted to pH 12 with NaOH and sonicated for 30 min at 60 ºC. Another centrifugation was performed and the sample was resuspended with previously prepared 100 mL pre-heated PEG dilution, adjusted and sonicated at same conditions. One last centrifugation step was performed and the pellets were washed with 20 mL Milli-Q water and stored at room temperature. Samples were studied by SEM, TEM and UV-Vis spectroscopy.

5.1.5 Functionalization of nanoparticles (NRs, NNs)

EDC and S-NHS stock solutions were obtained by dissolving a certain amount of each compound in one mL of Milli-Q water according to the total amount of gold to be functionalized following a proportion of 2 mg EDC and 4 mg S-NHS for each 1 mg of gold. The optimum gold amount is above 2 mg (generally around 4-10 mg in these experiments). The volume of nanoparticles containing the required amount of gold is concentrated by centrifugation at room temperature (3800 rpm 15 min for NNs and 13000 rpm 15 min for NRs) and resuspended in a total volume of 3 mL of 25 mM MES buffer pH 6, allowing it to fit into two Sephadex® columns. In the meantime, Sephadex® columns were equilibrated with the same buffer.

Both EDC and S-NHS were mixed together in a 2 mL Eppendorf tube and incubated 5 min ice cold. Then, the entire 2 mL volume was added to 3 mL solution containing the nanoparticles, and incubated 25 min undisturbed at room temperature to allow the intermediates to form. This was followed by dividing sample in two separate volumes of 2,5 mL each, that were passed through each of the columns and eluted with 3,5 mL 25 mM MES buffer pH 6 to discard unreacted molecules. The resultant elutions were collected and mixed together.

For the double-functionalized nanoparticles 0,5 mg of glucose and 0,2 mg TAMRA were prepared for each 1 mg of nanoparticles. These solutions were diluted separately in 1 mL Milli-Q water x10 times concentrated to allow a proper manipulation. They were added to the activated nanoparticles immediately after the elution of the columns and left incubating

overnight at room temperature protected from light and avoiding any disturbance. Once the reaction has finished, sample was loaded again into previously equilibrated Sephadex® columns and stored at 4 ºC protected from light. In order to produce single glucose-functionalized nanoparticles, previously reported protocol was applied except at TAMRA addition steps that should be skipped. Same proportions of glucose were added. Samples did not need to be protected from light. Samples were stored at 4 ºC. Prior use samples were concentrated at *ca.* x5 times by centrifugation at 3800 rpm 10 min for NNs and 7000 rpm 10 min for NRs both at room temperature.

5.2 Measurement of the heating capability

Both procedures were performed under working laser configuration (100%), in 96 well plates, in a total volume of 300 µL and with three readings per sample. Probe was washed and chilled down in Milli-Q water before each read. All stocks were firstly adjusted at two times concentration in Milli-Q water and later diluted to x1 in DMEM.

Heating trial 1 (**HT-I**) was performed by adding 150 µL of two-times concentrated nanoparticle stock solutions to 150 µL DMEM. All stocks prepared this way were adjusted to reach ABS_{LSPR} = 0.8. The entire 300 µL volumes were loaded into a 96 well plate leaving two empty wells between each sample. Three batches of optimized scaled-up protocol NR-D were studied together with one single batch of NNs synthesized with the 1000 nm protocol serving as positive control and an extra batch of NRs with LSPR at *ca.* 790 nm as negative control. A 1:1 dilution of Milli-Q-DMEM dilution was used as blank. Samples were irradiated for 4 min, registering temperature every 5 seconds. UV-Vis spectra were collected before and after irradiation.

Heating trial II (**HT-II**) was performed by preparing two times concentrated stock solutions in Milli-Q water and added 150 µL DMEM to get 50, 100 and 200 µg/mL final concentrations once loaded into the well. Both NNs and NRs were studied at the three concentrations, using 1:1 medium as blank and 200 µg/mL NR diluted in Milli-Q water as control. Samples were incubated undisturbed for 24h at 37 ºC with 5% CO_2 concentration, followed by irradiation for 5 min, registering temperature every 5 seconds. SEM images and UV-Vis spectra were collected from water-diluted stocks, before incubation and after and before and irradiation.

5.3 Studies of internalization of cells

5.3.1 Standard fluorescence microscopy

Ibidi inoculation protocol

Vero cells were cultured in µ-Dishes from Ibidi® (3.5 cm^2, ibiTreat coated for optimized adhesion) and cultured following factory protocols. $2x10^4$ cells were diluted in 400 µL of culture media and gently loaded to the plate. After 30 min incubation at 37 ºC with 5% CO_2, additional 1 mL DMEM was added to the plate and cultures were growth overnight at culture conditions. Medium was removed from the cells with a pipette and the cells were washed with PBS to remove excess medium before the addition of a sterilized suspension of nanoparticles funtionalized with glucose and TAMRA diluted in cell culture medium at a concentration of 0.2 mg/mL. Several hours after, cells were washed again and PBS was substituted by fresh medium. Samples were loaded into a culture visualization chamber with temperature control and visualized by fluorescence and phase contrast microscopy on a Nikon Eclipse Ti microscope.

5.3.2 Confocal microscopy

Sample preparation and cells fixation

The protocol of nanoparticles internalization and cell fixation was performed as follows: $2x10^4$ cells were seeded on a glass side cover inside a 24 well plate and growth for 24h at culture conditions. Medium was then substituted by a sterilized suspension of 0.2 mg/mL nanoparticles funtionalized with glucose and TAMRA diluted in medium and growth as described. Medium was then removed and cells were washed several times with *ca.* 500 µL DPBS under mild mixing to remove remaining nanoparticles. Last 500 µL DPBS were left 2-5 min incubating with cells. 4% p-formaldehyde was added to the cells and incubated ice-cold light-protected undisturbed for 20 min. P-formaldehyde was then removed by washing two times with DPBS and last 500 µL DPBS were left 2-5 min incubating with cells. DAPI addition was performed by adding 200 µL from a 1:50 stock dilution in DPBS and incubated 10 min at room temperature, followed by two washing steps with PBS or DPBS incubating 5 min between each step. DPBS was removed and Prolong® was then added by addition of *ca.* 6 µL pre-warmed (at room temperature) stock solution carefully turning over the cover on a slide. Samples were sealed by covering the perimeter of the slide cover containing cells with colorless nail varnish. Slides were stored at 4 ºC protected from light.

5.4. Using nanoparticles for optical hyperthermia with Class IV laser

5.4.1 Irradiation of Ibidi plates

Vero cells were cultured in μ-Dishes from Ibidi® following the same control as described elsewhere (see *Ibidi inoculation protocol* at *5.3.1 Standard fluorescence microscopy* section). After 24h growth, cells were supplemented with previously sterilized suspension of nanoparticles functionalized with glucose to a final concentration of 0.2 mg/mL. After 24h incubation under culture conditions, nanoparticles were washed with PBS and substituted with fresh media.

After washing sample, plates were irradiated under working laser configuration for 5 minutes, loaded into a culture visualization chamber with temperature control and visualized by phase contrast under a Nikon Eclipse Ti microscope.

5.4.2 Vero assay LIVE/DEAD Assay - NRs vs NNs

LIVE/DEAD® Assay from Invitrogen® was performed following kit indications to the letter. Cells were incubated in ibidi® treated plate for 24h under culture conditions before the addition of a suspension of 0.2 mg/mL of nanoparticles funtionalized with glucose diluted in culture media. Incubation with particles was carried out for 24h at culture conditions. Particles were removed and cells were cleaned few times with PBS supplemented with Mg^{2+} and Ca^{2+}. Before laser irradiation, live/dead® kit was added (250 μL per dish) with a concentration of 2.5 μM of EthD-1 and 5 μM of calcein AM in PBS supplemented with Ca^{2+} and Mg^{2+}. Cells were loaded into a culture visualization chamber with temperature control and incubated for 30 minutes at culture conditions before being irradiated for 5 min under working laser configuration. Fluorescence was observed under a Nikon Eclipse Ti microscope.